Advances in Science and Technology Research Journal

Advances in Science and Technology Research Journal, 18(7), 305–328
https://doi.org/10.12913/22998624/193197
ISSN 2299-8624, License CC-BY 4.0

Received: 2024.07.24
Accepted: 2024.09.11
Published: 2024.10.06

Drivetrain Modelling of Hybrid Electric Vehicles

Piotr Bera[1*]

[1] Department of Machine Design and Maintenance, Faculty of Mechanical Engineering and Robotics, AGH University of Krakow, al. A. Mickiewicza 30, 30-059 Kraków, Poland
E-mail: pbera@agh.edu.pl

ABSTRACT

The aim of this paper is to present mathematical models of all the propulsion components of hybrid drivetrains. These models are based on very limited amounts of data, nevertheless they match real characteristics with high accuracy based on numerous measurement data points, thus they allow the modelling process of fuel and energy consumption for a particular vehicle in any homologation driving cycle to be performed in a very short time at the early stage of vehicle design. The characteristics provided in the article concern: the full load engine torque curve, full load electric motor power curve, combustion engine efficiency characteristic, including dynamic states and warm-up period, electric motor efficiency characteristic, inverter efficiency characteristic, battery characteristics in a wide temperature range and efficiency of the drivetrain. Moreover, the main principles concerning gear ratio selection are provided to conduct subsequent steps of transmission modelling from scratch. Simulations of drivetrain performance and vehicle fuel consumption in WLTP and US06 tests prove the suitability of the presented models.

Keywords: hybrid drivetrain, brake specific fuel consumption, electric motor efficiency, battery efficiency, fuel consumption.

INTRODUCTION

The automotive industry is facing the difficult task of building cars with more powerful powertrains on the one hand, and using less fuel to meet the requirements imposed by the applicable standards on the other. CO_2 emissions from road vehicles contribute to the greenhouse effect and are recognized as a gas of which emissions should be significantly reduced. European Union regulations set CO_2 emission of passenger cars to 95 g/km in 2021 [1, 2]. Euro 7 [3, 4], which is planned to be introduced within a few years, will cut CO_2 limits even more. This forces vehicle manufacturers to produce more efficient cars, which means: increasing the efficiency of the internal combustion engine (ICE) [5, 6], implementation of transmissions that use 7, 8 or 9 gears [7], vehicle weight reduction [8], improving aerodynamics [9] or rolling resistance reduction. In the future, clean transport will be based mainly on battery electric vehicles, fuel cell electric vehicles [10, 11] and vehicles with hydrogen fuelled ICEs [12]. These vehicles are characterized by zero CO_2 road emissions. However, for now, there are still many problems concerning all of these groups. In the case of battery electric vehicles, they concern: range anxiety [13, 14], high price [15], performance at low temperature [16], high voltage lithium-ion traction battery (BAT) durability [17], availability of rare earth elements [18], peak energy demands influencing charging cost [19] or black out problems [20] due to overloaded energy systems. In the case of hydrogen vehicles, problems concern mainly methods of hydrogen production, the small number of hydrogen stations, vehicle prices, the small market of such vehicles and policy issues [21]. Another way to decrease CO_2 emissions significantly is with hybrid electric vehicle

(HEV), which refer to vehicles that use the ICE in conjunction with at least one electric motor (EM) and a BAT for propulsion. They are an area of interest of most car manufacturers, because they combine the advantages of battery electric vehicles and ICE-only drivetrains: mature technology, affordable prices, no range anxiety, zero emission driving at low speed, high durability and reliability. Some car manufacturers already have most models available as HEVs. This is the reason for continuous development of simulation methods of such drivetrains.

The full analysis of a hybrid drivetrain is very complex because it involves a few overlapping areas: mechanical design including e.g. gearing, ICE and EM characteristics, BAT performance characteristics and optimization algorithms that join all the above components together. These areas involve the analysis of many variables, interactions, and non-linear characteristics, requiring multidisciplinary teams equipped with professional software to solve series of single problems.

In [22], the authors studied the energy management of a power-split HEV equipped with planetary gear sets.

In [22], the authors studied the possibility of using alternative fuels as CNG, LPG and LNG, in combination with hybrid drive of a midibus, to quantitatively assess the further possibility of emissions reduction. In [23], the authors analyzed the function of a Hybrid Air system proposed in 2015 by PSA concern. It utilizes hydraulic components instead of electric ones in HEVs. Analysis concerning the modelling and optimization techniques of four types of hybrid powertrain configurations was conducted in [24]. An automated modelling method allowed 14 configurations to be classified based on a binary tree.

One paper [25] proposes a new optimal design approach of a permanent magnet synchronous motor in HEVs. It aims to solve the key research problem of how to find a viable and computationally efficient solution to achieve the maximum energy efficiency of the EM over the driving cycles.

The authors [26] present a thorough comparative study of energy management strategies for a parallel HEV, while BAT ageing is considered.

In [27], the authors estimated the operating time share of electric and hybrid modes in real driving conditions based on the electronically-controlled continuously variable transmission (e-CVT) series-parallel hybrid drivetrain. Analysis of the driver's operation allowed determination of the conditions of energy flow and the work share of the electric drive in the total driving time.

In [28, 29], the authors considered the influence of exploitation place and traffic control system on energy consumption, which is strongly connected with hybrid drivetrain programming and optimization. One element that significantly influences hybrid drivetrain functioning is the BAT. Its design influences size, efficiency and durability [16, 17, 30–33].

The articles mentioned above refer to drivetrain characteristics, but do not provide proper mathematical models of each component for the whole working range to perform the optimization process or verification of a particular drivetrain design, for example. Thus, the main aim of this article is to develop new formulas for the modelling of ICE, EM, BAT and inverter (INV), including the whole working range and a wide range of ambient temperature −10–40 °C. To carry out the whole modelling process, some basic formulas of vehicle dynamics, resistances, and ICE friction phenomena are also included.

To conduct the whole process of the drivetrain modelling along the manuscript, the following inputs are required: vehicle frontal area A_v [m^2], aerodynamic drag coefficient C_d[-], driven wheel dynamic radius R_d[m], empty vehicle mass m_e [kg] and maximum vehicle speed v_{max} [km/h]. As a result, the mileage fuel consumption G_V [dm^3/100 km] in any virtual homologation test, or at constant vehicle speed, is obtained.

The following sections present: the criteria of maximum gear ratio and the ratio of maximum speed, novel characteristics of ICE, EM, INV and BAT characteristics, simulations of fuel consumption and drivetrain performance in a Worldwide Harmonized Light-Duty Vehicles Test Procedure (WLTP) and US06 of vehicle with parallel hybrid drivetrain, proving the suitability of the proposed models of hybrid drivetrain components.

BASIC DRIVETRAIN CALCULATIONS

A vehicle body is always subjected to external and internal forces that make it move or keep it at a standstill, which is presented in Figure 1. For a vehicle in motion, the driving force F_{drv} must overcome rolling resistance force F_{roll}, aerodynamic drag force F_{aero}, inertia force F_{in} and grading force F_{slope}.

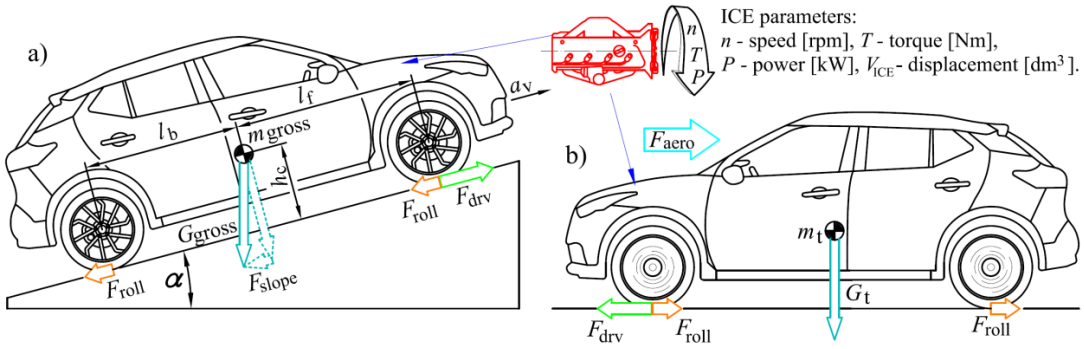

Figure 1. Forces acting on a vehicle

Maximum gear ratio

Moving off on a slope (Fig. 1a) determines the first gear total ratio i_{t1} in a parallel full-hybrid or just the reduction ratio in series and series-parallel hybrid for an EM. Every car must be capable of moving off on a slope of 26%. Formula (1) allowing a total ratio in first gear i_{t1} to be calculated concerns: fully loaded vehicle ($m_{gross} \approx 1.4 \cdot m_e$), front-wheel drive cars (which are most prone to tyre slipping), $\mu = 0.8$ (tyre-ground friction coefficient), $h_c = 0.5$ m, $l_b = l_f = 1.4$ m, vehicle acceleration $a_v = 0.8$ m/s^2 and $f_{roll} = 0.015$. Taking the above into consideration, the i_{t1} is:

$$i_{t1} > 3.4 \cdot \frac{m_{gross} \cdot R_d}{\eta_{tr} \cdot T_T} \tag{1}$$

Part of the power produced by the ICE or EM is lost due to the friction in the transmission, which is represented by η_{tr} in formula (1). In the initial drivetrain calculations the following values can be used [34–36]: $\eta_{tr} \approx 90\%$ for automated mechanical transmission (AMT) and dry dual clutch transmission (DCT), $\eta_{tr} \approx 87\%$ for wet DCT, $\eta_{tr} \approx 83\%$ for automatic transmission (AT) and e-CVT.

The second factor concerns dry friction clutch durability (in the case of AMT and dry DCT). The i_{t1} ratio should be relatively high to ensure nominal clutch durability of 250 000 km. For a standard clutch material [37, 38], 50% of city driving with 3 starts/1 km, 50% of extra-urban driving with 0.2 starts/1 km, 2% of uphill starts ($\alpha = 15\%$), average vehicle load is half of the maximum load [36, 39] ($m_t \approx 1.2 \cdot m_e$) and $n_{ICE} \approx 1500$ rpm, the following formula for i_{t1} was developed:

$$i_{t1} > 0.0042 \cdot R_d \cdot n_{ICE} \cdot \sqrt{m_t} \Big/ \sqrt[3]{T_T} \tag{2}$$

In the case of series and series-parallel drivetrains, i_{t1} must also meet the condition of maximum speed v_{max} for traction EM which is permanently connected to the wheels and its speed cannot usually exceed 15 000 rpm [40].

Maximum vehicle speed

The maximum speed v_{max} [km/h] of a vehicle (Fig. 1b) is a constant speed that can be developed on a flat, dry road, without wind, with the throttle fully opened. In the case of a hybrid vehicle, v_{max} is calculated for the power of the ICE only:

$$[0.5 \cdot \rho_{air} \cdot C_d \cdot A_v \cdot (v_{max}/3.6)^2 + m_t \cdot g \cdot f_{roll}] \cdot v_{max}/3600 = P_{ICE}(n_{vmax}) \cdot k_{chg} \cdot \eta_{tr} \tag{3}$$

The maximum speed v_{max} is reached at ICE speed $n_{vmax} = (0.90–1.05) \cdot n_N$ (according to Table 1). The coefficient $k_{chg} = (0.95–0.98)$ takes into account the need for BAT recharging, after depletion during acceleration to v_{max}. In the initial calculation, ICE power $P_{ICE}(n_{vmax}) \approx P_N$ [kW] can be assumed. Tyre rolling resistance coefficient f_{roll} can be calculated based on Kamm model [41].

Then the gear number (AMT, AT and DCT) for v_{max} (3) is set based on Figure 2 (Input data for the example marked with blue lines are: $P_N = 53$ kW and normal version. This results in a 5-speed gearbox, v_{max} is reached in $k = 4^{th}$ gear and $k_v = 0.95$).

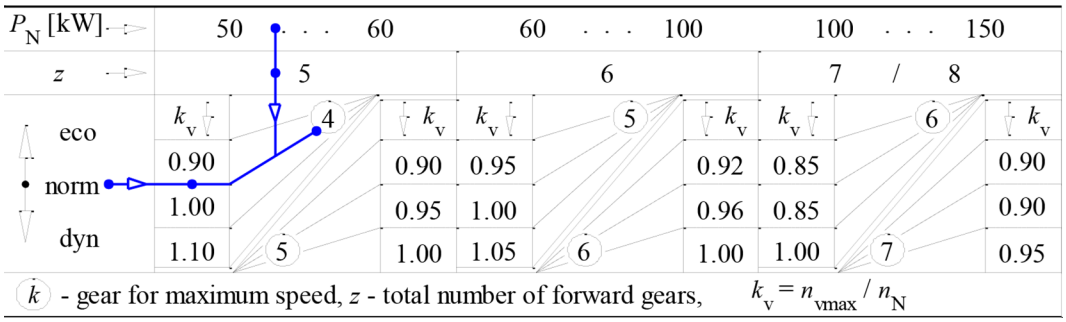

Figure 2. Selection of drivetrain parameters with regard to desired vehicle characteristics

In the case of AMT, AT and DCT, intermediate gears and overdrive must also be calculated [36], whereas in the case of series-parallel e-CVT transmissions, the geometry of planetary gears must also be determined [33, 42].
Now, when the nominal ICE power P_N is known, other ICE parameters: ICE displacement V_{ICE} [dm^3]:

$$V_{ICE} = \frac{120 \cdot P_N}{n_N \cdot C_{NT} \cdot bmep(n_T)} \tag{4}$$

and ICE nominal torque T_T [Nm] developed at n_T:

$$T_T = \frac{bmep(n_T) \cdot V_{ICE}}{0.01256} \tag{5}$$

can be determined with the use of data from Table 1.

Table 1. Basic parameters of spark ignition (SI) ICEs used in hybrid drivetrains

No	Parameter	SI NA Atkinson	SI NA Otto	SI TB Otto	SI Miller (charged)
1	$bmep(n_T)$ [MPa]	1.0–1.1	1.2–1.3	1.8–2.5	1.5–1.8
2	n_T [rpm]	3000–4000	3500–5000	1400–2500	1400–4400
3	n_N [rpm]	5000–6000	5000–6300	4500–6000	5000–5500
4	C_{NT} [-]*	0.80–0.95	0.70–0.90	0.70–0.90	0.85–0.90

Note: *smaller value for greater n_N, greater value for smaller n_N and when $bmep(n_M)$ is small, NA – naturally aspirated, TB – turbocharged.

INTERNAL COMBUSTION ENGINE

ICE torque and power characteristics

In full-hybrid drivetrains SI Atkinson cycle ICEs are commonly used. They are characterized by a long piston stroke (γ = cylinder bore B [mm] / piston stroke S [mm] < 0.8) and late intake valve closing. Mild-hybrid drivetrains are usually equipped with NA Otto ICEs or SI TB ICEs. The parameters allowing (6) to be calculated are presented in Table 1. In the proposed ICE model (6), the power P [kW] and torque T [Nm] characteristics versus rotational speed n with the throttle fully opened (Fig. 3) are based on 5 highlighted points.

The developed formula (6) can be used both for ICEs where the peak torque T_T occurs at one speed as well as in a wide speed range (n_{T1}-n_{T2}):

$$T(n) = -a_0 \cdot |n - n_0|^p + T_T \tag{6}$$

where the coefficients depending on n are:

$$n_0 = \frac{n_{T2} - n_{T1}}{1 + 0.5\text{^}\left[n - 0.5 \cdot \left(n_{T1} + n_{T2}\right)\right]} + n_{T1} \tag{7}$$

$$a_0 = \left[\frac{-a_1}{1 + 0.01\text{^}\left(n - n_{T1}\right)} + a_1 + \frac{a_2}{1 + 0.01\text{^}\left(n - n_{T2}\right)}\right] \tag{8}$$

$$p = \frac{p_2 - p_1}{1 + 0.5\text{^}\left[n - 0.5 \cdot \left(n_{T1} + n_{T2}\right)\right]} + p_1 \tag{9}$$

and the constants:

$$p_1 = \frac{\ln\left[\left(T_m - T_T\right)/\left(T_{idle} - T_T\right)\right]}{\ln\left[\left(n_{T1} - n_m\right)/\left(n_{T1} - n_{idle}\right)\right]} \tag{10}$$

$$a_1 = \frac{T_T - T_{idle}}{\left(n_{T1} - n_{idle}\right)\text{^}\,p_1} \tag{11}$$

$$T_N = 9550 \cdot P_N / n_N \tag{12}$$

$$p_2 = \frac{T_N \cdot \left(n_N - n_{T2}\right)}{n_N \cdot \left(T_T - T_N\right)} \tag{13}$$

$$a_2 = \frac{T_T - T_N}{\left(n_N - n_{T2}\right)\text{^}\,p_2} \tag{14}$$

To evaluate the accuracy of the presented model (6) and further models: (17), (62) and (86), they are compared with real characteristics. The difference Δ is defined as:

$$\Delta = \frac{S - M}{S} \cdot 100\% \tag{15}$$

where: S determines the series parameter and M determines the model parameter. The parameter S is torque, efficiency or voltage, with regard to the analysed model. Table 2 presents a comparison of serial characteristics with their models based on (6).

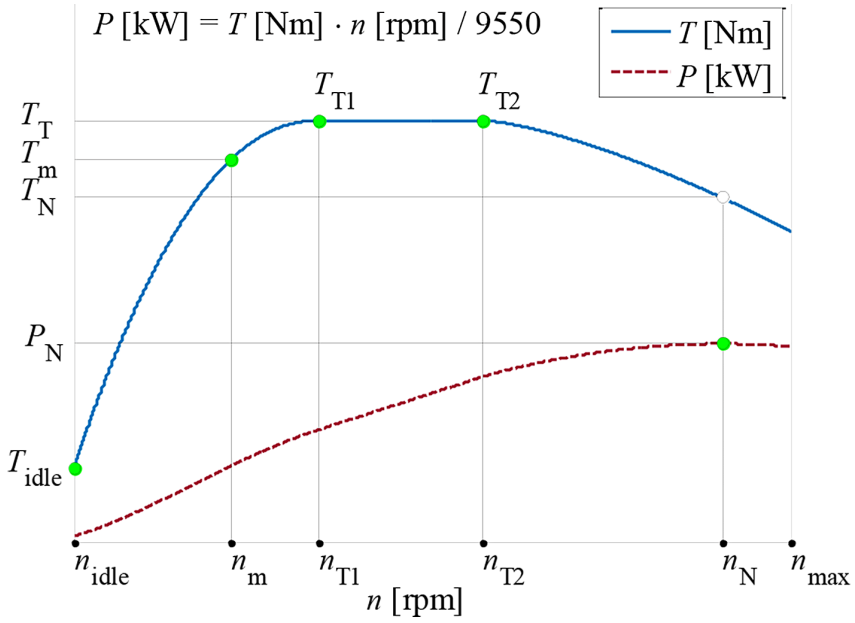

Figure 3. ICE power and torque performance curves

Table 2. Comparison of serial characteristics with their models based on (18)

Parameter	Mazda 2.0 Skyactiv-G	Toyota 2.5 D-4S	VW 1.5 TSI evo
Serial	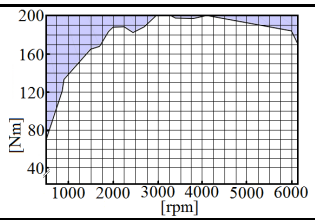	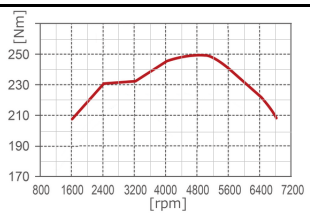	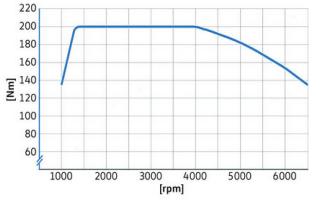
Model	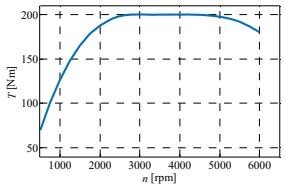	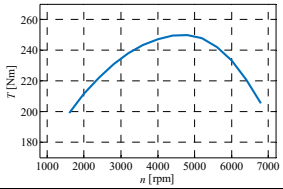	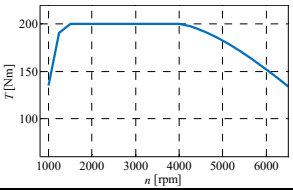
Δ [%]	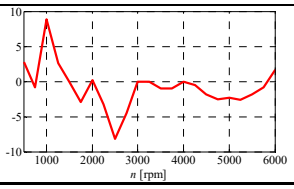	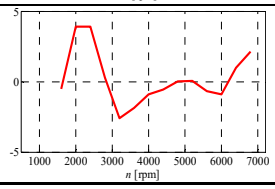	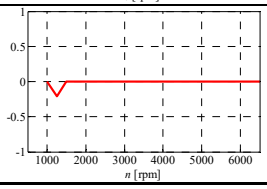

It can be noticed that the difference Δ strongly depends on the original shape of the torque characteristic. In the case of properly drawn (without irregularities) original torque, the maximum difference is $|\Delta| < 0.2\%$ (VW 1.5 TSI evo).

Brake specific fuel consumption characteristic

The overall ICE efficiency reaches over 40% for SI Atkinson cycle ICEs. This parameter is sometimes presented in the form of η_{ICE} contours in a coordinate system of n and T. It can also be presented as a brake specific fuel consumption g_e [g/kWh] characteristic (Fig. 4). The η_{ICE} and g_e can be used interchangeably (petrol calorific value $W_p = 43$ MJ/kg [43]):

$$\eta_{ICE} = (84 / g_e) \cdot 100\% \tag{16}$$

The parameters allowing (17) to be calculated are presented in Table 3.

Table 3. Parameters of SI ICEs required for a g_e characteristic

No	Parameter	SI NA Atkinson	SI NA Otto	SI TB Otto	SI Miller (charged)
1	*CR* [-]	13.0–14.0	10.8_{MPI}–11.0_{GDI}	10.0_{MPI}–10.5_{GDI}	< 12.5
2	η_{P0} [%]	41	38	36	38
3	T_{P0} [Nm]	$(0.6–0.8)\cdot T_T$	$(0.6–0.8)\cdot T_T$	$(0.6–0.7)\cdot T_T$	$(0.7–0.8)\cdot T_T$
4	n_{P0} [rpm]	1700-2500	2500-3000	2000-3000	2000-3000
5	T_{P1} [Nm]	$\sim 0.15\cdot T_T$	$\sim 0.15\cdot T_T$	$\sim 0.15\cdot T_T$	$\sim 0.15\cdot T_T$
6	η_{P1} [%]	$\sim 0.6\cdot \eta_{P0}$	$\sim 0.55\cdot \eta_{P0}$	$\sim 0.7\cdot \eta_{P0}$	$\sim 0.7\cdot \eta_{P0}$
7	η_{P2} [%]	$\sim (0.85–0.95)\cdot \eta_{P0}$			
8	λ_k [-]	~ (0.90–0.95)			
9	λ_m [-]	~ (0.85–0.90)			

Note: points: 2–7 – see Fig. 4, *MPI* - multipoint port injection, GDI - gasoline direct injection, *CR* – compression ratio.

The formula for η_{ICE} (17) requires η, n and T of 5 highlighted points: $P_0 \ldots P_4$. Maximum efficiency η_{P0} is reached at P_0. Points $P_0 \ldots P_5$ are located so as to match real contour shapes. The dashed green line represents the optimum operating curve.

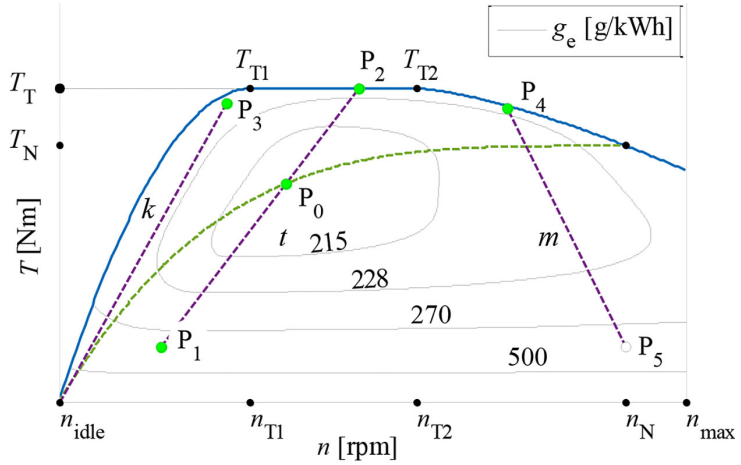

Figure 4. Brake specific fuel consumption characteristic

The developed formula for η_{ICE} in the whole working range is the following:

$$\eta_{ICE} = -\left[\frac{(\eta_t - \eta_m)/(n_t - n_m)^2 - (\eta_t - \eta_k)/(n_t - n_k)^2}{1 + 0.01\hat{}(n - n_t)} + \frac{\eta_t - \eta_k}{(n_t - n_k)^2}\right] \cdot (n - n_t)^2 + \eta_t \tag{17}$$

where: the variables depending on the torque T are:

$$\eta_t = \left[\frac{a_{td} - a_{tg}}{1 + 0.01\hat{}(T - T_{P0})} - a_{td}\right] \cdot |T - T_{P0}| \hat{} \, p_t + \eta_{P0} \tag{18}$$

$$n_t = (T - T_{P1}) \cdot \frac{n_{P0} - n_{P1}}{T_{P0} - T_{P1}} + n_{P1} \tag{19}$$

$$\eta_k = \eta_t \cdot \lambda_k \tag{20}$$

$$n_k = T \cdot \frac{n_{P3} - n_{idle}}{T_{P3}} + n_{idle} \tag{21}$$

$$\eta_m = \eta_t \cdot \lambda_m \tag{22}$$

$$n_m = (T - T_{P5}) \cdot \frac{n_{P4} - n_{P5}}{T_{P4} - T_{P5}} + n_{P5} \tag{23}$$

and the constant values connected with line t:

$$p_t = \frac{\ln[(\eta_{P0} - \eta_{P1})/\eta_{P0}]}{\ln[(T_{P0} - T_{P1})/T_{P0}]} \tag{24}$$

$$a_{td} = \eta_{P0} / (T_{P0} \hat{} \, p_t) \tag{25}$$

$$a_{tg} = \frac{\eta_{P0} - \eta_{P2}}{(T_{P2} - T_{P0}) \hat{} \, p_t} \tag{26}$$

The presented model of ICE efficiency (17) is now compared with characteristics provided by vehicle manufacturers. In contrary to model (17), which is based on 6 points, original characteristics are usually based on more than 400 points. Table 4 presents 3 serial characteristics of η for SI ICEs, their corresponding models, and relative error Δ according to (15). To determine the difference graph, serial characteristics were meshed as presented in the first line of Table 4: the ICE speed step is 250 rpm and the torque step is 10 Nm.

Table 4. Comparison of serial η characteristics with their models based on (17)

Parameter	Honda 1.5 L15B7	Mazda 2.0 Skyactiv-G	Toyota 2.5 A25A-FKS
Serial	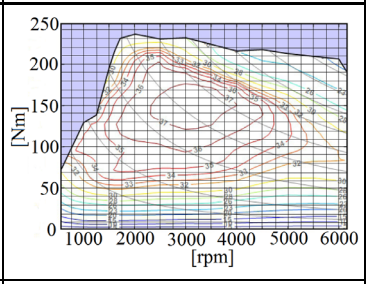	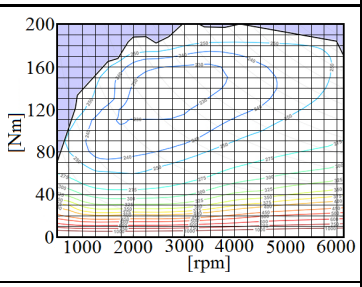	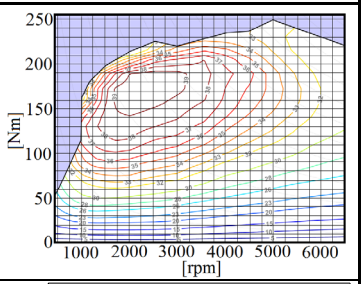
Model	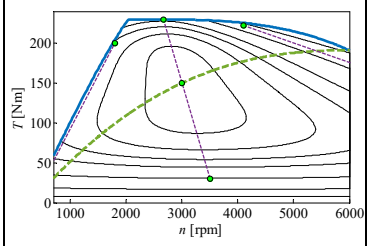	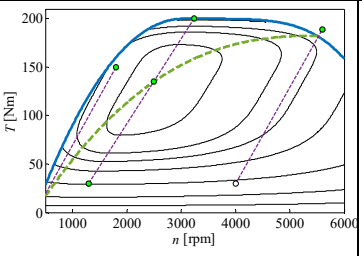	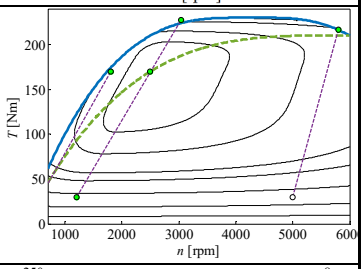
Δ [%]	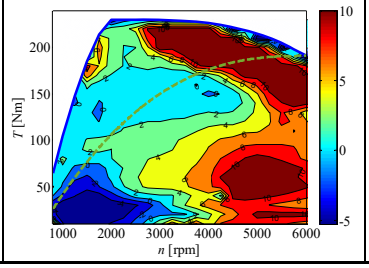	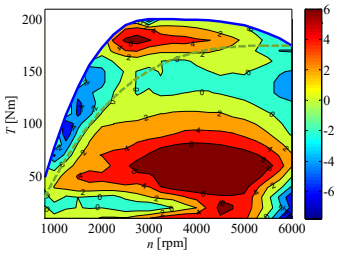	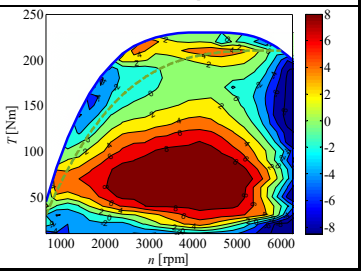

The error Δ along the optimum operating curve does not exceed ± 4% in the case of NA ICEs (Mazda and Toyota). Higher values of error Δ (Mazda and Toyota), of no more than ± 6%, are obtained at low load and high speed – which is the area where ICEs do not usually work. The results show that the proposed model better fits NA ICEs, where λ is stoichiometric in a much wider area than in the case of TB ICEs, which creates sudden changes in g_e at high load (Honda). In this case, the error Δ along the optimum operating curve reaches 10%.The above characteristic (17) allows the calculation of a g_e in steady states (when n and T are constant) and at a nominal working temperature, which is usually about 90 °C. Formula (27) allows G_V [dm^3/100km] for a constant v [km/h], also during the warm-up period (the ICE temperature influences the equivalence ratio $\lambda(temp_{ICE})$ (53) and oil viscosity influences friction torque (29), (47)), to be calculated:

$$G_v = 1.05 \cdot \frac{g_e(n, T_{dyn})}{\lambda(temp_{ICE})} \cdot \frac{T_{dyn} \cdot n}{v \cdot \rho_{fuel}} \cdot 10^{-5} \tag{27}$$

and $\rho_{fuel} = 0.75$ g/cm^3. The calculation of idle fuel consumption G_h [dm^3/h] (28) needs a small torque to be assumed, e.g., $T = 0.1$ Nm (at $T = 0$ Nm g_e cannot be calculated). Then the formula is:

$$G_h = 1.05 \cdot \frac{g_e(n_{idle}, T)}{\lambda(temp_{ICE})} \cdot \frac{T \cdot n_{idle}}{\rho_{fuel}} \cdot 10^{-7} \tag{28}$$

Dynamic states

The ICE used for vehicle propulsion works permanently in highly dynamic working conditions. A detailed model, based on artificial neural networks, can be used [44, 45] to represent the dynamic behaviour of the ICE. It includes inertias of rotating components as well as inertia of the oil and coolant. The delay in the ICE response to a control signal is also included. However, such a model requires plenty of detailed data concerning the particular ICE. Thus, commonly static ICE characteristics, with the inclusion of ICE inertia J_{ICE} [kg·m^2], are used to represent ICE dynamics and specific fuel consumption

[33, 34, 36, 39, 46, 47]. In this article, the following model of ICE behaviour in dynamic states is proposed:

$$T_{dyn} = T - T_{fr\_v} - J_{ICE} \cdot \varepsilon_{ICE} \cdot \left[1 + k_{nm} \cdot \mathrm{sgn}(\varepsilon_{ICE})\right] \tag{29}$$

where: the developed formula for ICE inertia is J_{ICE}:

$$J_{ICE} = 0.1 \cdot (V_{ICE}^2 - V_{ICE} + 1) \tag{30}$$

The coefficient $k_{nm} < 0.01$ takes into account non-mechanical inertias of the oil and coolant. T_{fr_v} is the friction torque (47) generated by the oil when $temp_{oil} < 100$ °C.

Warm-up period

When a cold ICE starts at an ambient temperature $temp_{amb}$ it consumes much more fuel than at a nominal working temperature because of the increased oil viscosity and air-fuel mixture (AFM) enrichment. Determination of heat phenomena during the warm-up time is important in overall G_V analysis and has been investigated in many research projects [48–54].

In the following analysis, it is assumed that ICE temperature $temp_{ICE}$ represents: block, head, pistons (made of aluminium) and coolant temperature, whereas oil temperature $temp_{oil}$ represents the temperature of oil, crankshaft and oil pan. Heat and cooling sources in the ICE are presented in Figure 5. The energy for the ICE propulsion H_{AFM} [W] comes from the AFM [43, 48] flowing into cylinders. With regard to petrol calorific value this energy equals:

$$H_{AFM} = 12 \cdot g_e \cdot P \tag{31}$$

After a cold start, part of H_{AFM} warms up the ICE [43, 48, 55]:

$$H_{IN} = 1.33 \cdot n^{0.46} \cdot H_{AFM}^{0.51} \tag{32}$$

Part of H_{IN} [W] is transferred from the coolant to the cabin heat exchanger:

$$H_{che} = 10^{-3} \cdot h_{che} \cdot V_{che} \cdot \beta_{che} \cdot \left(temp_{ICE} - temp_{amb}\right) \tag{33}$$

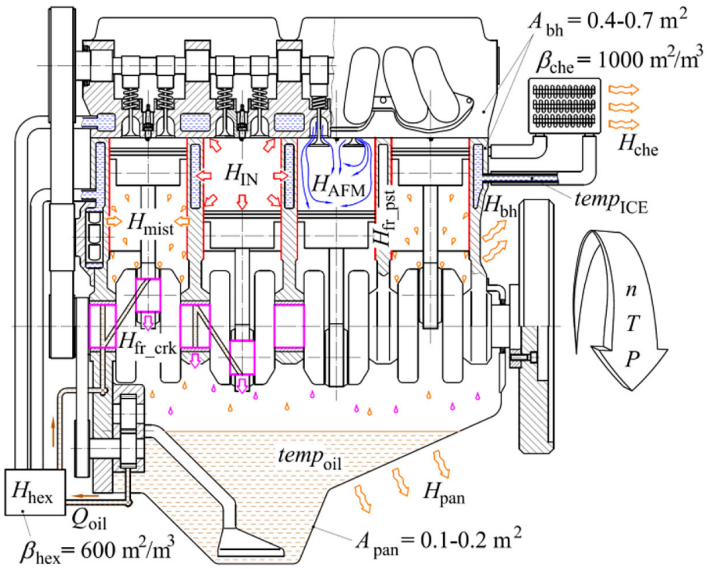

Figure 5. Heat transfer in the ICE

Heat is also given away to the surroundings through the cylinder block and head, cooled by the air flowing by:

$$H_{bh} = A_{bh} \cdot h_{bh} \cdot \left(temp_{ICE} - temp_{amb}\right) \tag{34}$$

Part of H_{IN} is transferred from the coolant to the oil in the heat exchanger:

$$H_{hex} = 10^{-3} \cdot h_{hex} \cdot V_{hex} \cdot \beta_{hex} \cdot \left(temp_{ICE} - temp_{oil}\right) \tag{35}$$

Oil is also warmed-up by contact with hot ICE parts. This heat depends on the total oil pump flow Q_{oil} [kg/s] in the ICE [43, 56–59], which can be described by the following, developed model:

$$Q_{oil} = 9.2 \cdot 10^{-11} \cdot P_N \cdot \left(n / n_N\right)^{0.625} \cdot \left(temp_{oil} + 50\right)^{3.5} \tag{36}$$

By means of splash lubrication, part of the total input heat [57, 60–64] is transferred to an oil mist H_{mist} [W] in a crankcase:

$$H_{mist} = 0.2 \cdot C_{oil} \cdot Q_{oil} \cdot \left[temp_{ICE} + \left(10 + 50 \cdot P / P_N\right) - temp_{oil}\right] \tag{37}$$

Another part of heat is transferred from the ICE block to the oil when it is in the valve-train area and then flows down to the oil pan:

$$H_{cam} = 0.02 \cdot C_{oil} \cdot Q_{oil} \cdot \left(temp_{ICE} - temp_{oil}\right) \tag{38}$$

The heat H_{pan} that the oil transfers through the oil pan to the air increases with v and is:

$$H_{pan} = A_{pan} \cdot h_{pan} \cdot \left(temp_{oil} - temp_{amb}\right) \tag{39}$$

Moreover, part of the H_{AFM} (31) is used to overcome the ICE inside friction. This is an important part of energy loss (mainly in the area of crankshaft bearings and piston-cylinder assembly), which plays an important role in ICE warm-up, and generates additional resistance torque T_{fr_v} [Nm] (47). It can be calculated precisely according to [65, 66]. Characteristics of the most common ICE oils [67] used in full-hybrid drivetrains are presented in Table 5.

Table 5. Specifications of 0W-16, 0W-20 and 5W-30 oils

Oil	v(40 °C) [mm²/s]	v(100 °C) [mm²/s]	k_{oil} [mm²/s]	Θ_1 [°C]	Θ_2 [°C]
0W-16	29.9	6.7	0.125	871.9	119.7
0W-20	44.9	8.6	0.129	889.6	112.5
5W-30	66.4	11.7	0.088	1116	129.0

Note: $v(temp_{oil}) = k_{oil} \cdot \exp[\theta_1/(\theta_2 + temp_{oil})]$.

All the *fmep* [kPa] factors, connected with mechanical friction phenomena in the area of the crankshaft (crk), pistons (pst) and camshafts (cam), are the following [43, 65]:

$$fmep_{total} = \sqrt{\frac{v(temp_{oil})}{v(100^{o}\mathrm{C})}} \cdot \left[fmep_{crk1}(v) + fmep_{pst1}(v) + fmep_{cam1}(v)\right] + \left(fmep_{crk2} + fmep_{pst2} + fmep_{cam2}\right) \tag{40}$$

where:

$$fmep_{crk1}(v) = 3.03 \cdot 10^{-4} \cdot n \cdot B \cdot \gamma \cdot \left[0.129 \cdot \left(n_c + 1\right)/ n_c + 0.096\right] \tag{41}$$

$$fmep_{crk2} = 0.85 \cdot 10^{5} \cdot \gamma / \left(B^2 \cdot n_c\right) + 0.66 \cdot 10^{-10} \cdot B^2 \cdot n^2 \cdot \left(n_c + 1\right)/ n_c \tag{42}$$

$$fmep_{pst1}(v) = 0.0098 \cdot n / \gamma + 4 \cdot T \cdot bmep(n_T)/ T(n) + 2.07 \tag{43}$$

$$fmep_{pst2} = \frac{3.66 \cdot 10^{4}}{B^2} \cdot \left(1 + \frac{500}{n}\right) + \left[0.7 \cdot bmep(n_T) \cdot \frac{T}{T(n)} + 0.36\right] \cdot \left[CR\text{^}\left(1.33 - \frac{9.33 \cdot n \cdot B}{10^{7} \cdot \gamma}\right)\right] \tag{44}$$

$$fmep_{cam1}(v) = 84 \cdot [5.08 \cdot n \cdot \left(n_c + 2\right) \cdot \gamma / \left(B^3 \cdot n_c\right) + \sqrt{n} \cdot \gamma / B^2] \tag{45}$$

where: n_c is the number of cylinders. The cylinder bore B [mm], can be calculated in the following way:

$$B = 108.4 \cdot \sqrt[3]{\gamma \cdot V_{\mathrm{ICE}} / n_{\mathrm{c}}} \tag{46}$$

The factor $fmep_{\mathrm{cam2}}$ including friction factors connected with valve-train design independent of oil viscosity can be ignored, because it is small, and it is difficult to differentiate the heat from the valve-train from combustion heat. The efficiency characteristic (Fig. 4) includes oil friction when the ICE and oil have nominal working temperatures. Thus, to calculate fuel consumption (27)–(28) and dynamics (29) at lower oil temperature, only factors dependent on oil viscosity are considered:

$$T_{\mathrm{fr}\_\nu} = \frac{V_{\mathrm{ICE}}}{12.56} \cdot \left\{ \sqrt{\frac{k_{\mathrm{oil}} \cdot \exp\left[\theta_1 / (\theta_2 + temp_{\mathrm{oil}})\right]}{\nu(100^{\mathrm{o}}\mathrm{C})}} - 1 \right\} \cdot \left[fmep_{\mathrm{crk1}}(\nu) + fmep_{\mathrm{pst1}}(\nu) + fmep_{\mathrm{cam1}}(\nu) \right] \tag{47}$$

However, in the case of calculations of ICE warm-up, it is the total piston friction $H_{\mathrm{fr\_pst}}$ [W] which warms up the coolant:

$$H_{\mathrm{fr\_pst}} = \frac{V_{\mathrm{ICE}} \cdot n}{120} \cdot \left\{ \sqrt{\frac{k_{\mathrm{oil}} \cdot \exp\left[\theta_1 / (\theta_2 + temp_{\mathrm{oil}})\right]}{\nu(100^{\mathrm{o}}\mathrm{C})}} \cdot fmep_{\mathrm{pst1}}(\nu) + fmep_{\mathrm{pst2}} \right\} \tag{48}$$

and the total crankshaft friction $H_{\mathrm{fr\_crk}}$ [W] which warms up the oil:

$$H_{\mathrm{fr\_crk}} = \frac{V_{\mathrm{ICE}} \cdot n}{120} \cdot \left\{ \sqrt{\frac{k_{\mathrm{oil}} \cdot \exp\left[\theta_1 / (\theta_2 + temp_{\mathrm{oil}})\right]}{\nu(100^{\mathrm{o}}\mathrm{C})}} \cdot fmep_{\mathrm{crk1}}(\nu) + fmep_{\mathrm{crk2}} \right\} \tag{49}$$

The calculations of ICE warm-up requires its mass m_{ICE} [kg], which is:

$$m_{\mathrm{ICE}} = (40 \cdot V_{\mathrm{ICE}} + 35) \cdot k_{\mathrm{ICE}} \tag{50}$$

where: $k_{\mathrm{ICE}} = 1.0$ for NA ICE and $k_{\mathrm{ICE}} = 1.2$ for TB ICE. Table 6 presents the specifications of materials and elements required for ICE warm-up calculations.

Taking the above into consideration, the oil temperature changes according to:

$$\Delta temp_{\mathrm{oil}} = \frac{H_{\mathrm{mist}} + H_{\mathrm{fr\_crk}} + H_{\mathrm{hex}} + H_{\mathrm{cam}} - H_{\mathrm{pan}}}{C_{\mathrm{oil}} \cdot \rho_{\mathrm{oil}} \cdot V_{\mathrm{oil}} + k_{\mathrm{add}} \cdot C_{\mathrm{crk}} \cdot m_{\mathrm{crk}} + C_{\mathrm{pan}} \cdot m_{\mathrm{pan}}} \cdot \Delta t \tag{51}$$

where: $k_{\mathrm{add}} = 1.2$ includes additional mass of the crankshaft support. The ICE temperature change in the time interval Δt [s] is:

$$\Delta temp_{\mathrm{ICE}} = \frac{H_{\mathrm{IN}} + H_{\mathrm{fr\_pst}} - H_{\mathrm{che}} - H_{\mathrm{mist}} - H_{\mathrm{bh}} - H_{\mathrm{hex}} - H_{\mathrm{cam}}}{C_{\mathrm{bh}} \cdot m_{\mathrm{bh}} + C_{\mathrm{pst}} \cdot m_{\mathrm{pst}} + k_{\mathrm{sc}} \cdot C_{\mathrm{clnt}} \cdot \rho_{\mathrm{clnt}} \cdot V_{\mathrm{clnt}}} \cdot \Delta t \tag{52}$$

where: $k_{\mathrm{sc}} \approx 30\%$ is the part of total coolant volume in a small circuit. The equivalence ratio λ during the warm-up period depends on $temp_{\mathrm{ICE}}$ and can be assessed by the developed formula:

$$\lambda(temp_{\mathrm{ICE}}) = \left[1.7 - \frac{0.7}{1 + \exp(-0.08 \cdot temp_{\mathrm{ICE}})} \right]^{-1} \tag{53}$$

After ICE start-up at an ambient temperature, it usually works permanently until it reaches at least 40 °C. Then a stop-start function is activated.

The above thermal model of the ICE is used in simulations in Validation of hybrid transmission models section, where the ICE works under load, according to traffic conditions. These simulations indicate the maximum difference of 8% between the proposed model and real ICEs.

Table 6. Specifications of ICE materials and parts (average values)

Part name ($_{abbr.}$)	ρ [kg/m^3]	V [dm^3]	m [kg]	C [J/(kgK)]	h [W/(m^{2}K)]
Oil ($_{oil}$)	850	4–5	$10^{-3}\cdot\rho_{oil}\cdot V_{oil}$	1985	-
Coolant ($_{clnt}$)	1070	5–9	$10^{-3}\cdot\rho_{clnt}\cdot V_{clnt}$	3300	-
Cabin heat exch.[1]($_{che}$)	2700	1.0–1.8	-	930	0-30
Oil heat exch.[1] ($_{hex}$)	2700	$0.3\cdot V_{ICE}$	-	930	300
Block, head[1] ($_{bh}$)	2700	-	$25\%\cdot m_{ICE}$	930	$5+12\cdot v^{0.25}$
Pistons[1] ($_{pst}$)	2700	-	$1.2\%\cdot m_{ICE}$	930	-
Oil pan[1] ($_{pan}$)	2700	-	$2\%\cdot m_{ICE}$	930	$5+12\cdot v^{0.25}$
Crankshaft[2] ($_{crk}$)	8750	-	$12\%\cdot m_{ICE}$	490	50

ICE start

In a hybrid drivetrain, the ICE is permanently stopped and started. A quick response to provide an immediate reaction to the driver demands results in a high angular acceleration of the EM and ICE connected together by means of a gear pair. When the ICE is stopped, the EM acts as a starter and uses electric energy supplied from the BAT to put the ICE into motion. In the ICE start process, the EM must overcome its own inertia (78) and ICE resistances: inside friction, inertia, pressure loading and pumping losses. To ensure a quick and smooth start, the ICE must reach n_{idle} in about 0.3 s [68, 69], which results in an angular acceleration of $\varepsilon_{ICE} \approx 300$ rad/s^2. The peak power required to start the ICE is:

$$P_{ICE\_start} = \frac{T_{ICE\_start}\cdot n_{idle}}{9550} = \frac{\left(J_{ICE}\cdot\varepsilon_{ICE} + k_{start}\cdot V_{ICE}\right)\cdot n_{idle}}{9550} \tag{54}$$

where: k_{start} is:

$$k_{start} = v(100^{o}\text{C})\cdot\left[0.965\text{^}\left(temp_{oil}+5\right)\right]+11.5 \tag{55}$$

The developed coefficient k_{start} varies significantly with oil temperature, e.g. for 0W-20 oil: k_{start} = (22, 12) for (-10 °C, 90 °C) respectively.

ELECTRIC MOTOR

Electric motor torque characteristic

EM is a better propulsion for automotive vehicles than the ICE due to its numerous advantages: small size (high power and torque density), perfect balance, high speed range (in automotive applications EMs reach a maximum speed of 15 000 rpm [40]), high torque from zero speed and high efficiency (over 97% [40]) in a wide range of work field. To draw graphs of P and T (Fig. 6) specific parameters for highlighted points must be provided.

The developed formula allows P in the whole range of n to be calculated:

$$P(n) = -a_0\cdot\left|n-n_0\right|^{p} + P_N \tag{56}$$

where the variables are the following:

$$n_0 = \frac{n_N - n_{Tmax}}{1+0.5\text{^}\left[n-0.5\cdot\left(n_{Tmax}+n_N\right)\right]} + n_{Tmax} \tag{57}$$

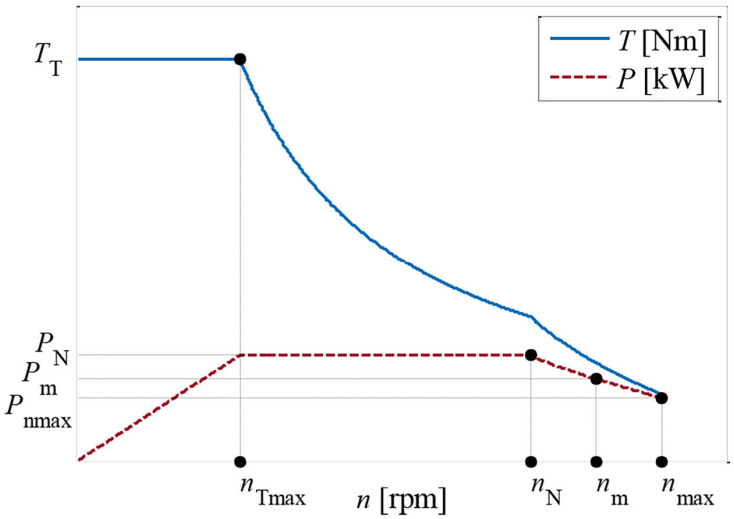

Figure 6. EM power and torque characteristics

$$a_0 = \left[\frac{-P_N / n_{T\max}}{1 + 0.01\text{^}\left(n - n_{T\max}\right)} + \frac{P_N}{n_{T\max}} + \frac{a_2}{1 + 0.01\text{^}\left(n - n_N\right)} \right] \tag{58}$$

$$p = \frac{p_2 - 1}{1 + 0.5\text{^}\left[n - 0.5 \cdot \left(n_{T\max} + n_N\right)\right]} + 1 \tag{59}$$

and the constants:

$$p_2 = \frac{\ln\left[\left(P_N - P_{n\max}\right)/\left(P_N - P_m\right)\right]}{\ln\left[\left(n_{\max} - n_N\right)/\left(n_m - n_N\right)\right]} \tag{60}$$

$$a_2 = \frac{P_N - P_m}{\left(n_m - n_N\right)\text{^}\, p_2} \tag{61}$$

The above formula can be used in calculations of vehicle dynamics, e.g. acceleration time, which requires the inclusion of EM inertia (77)–(78).

Electric motor efficiency characteristic

An EM is characterised by high efficiency in the whole work area, with the maximum value exceeding 97%. This section allows a formula for motor efficiency, as a function of its speed n and torque T, to be determined. The developed formula (62) is based on 14 highlighted points (Fig. 7), which should come from measurements performed on a test rig. Each point P_0–P_9 is determined by 3 values: n, T and η (except P_4 which requires only speed: n_{P4}). The specific conditions that allow the use of (62) are: $n_{P7} = n_{P8} = n_{P9} = n_w$, $T_{P7} = T_{P1}$, $T_{P8} = T_{P0}$, $T_{P9} = T_{P2}$, $T_{P1} < 0.5 \cdot T_{P0}$, $T_{P3} = T_{P5} = T_{P6} = T_T$, points: P_{kd}, P_{ku}, P_{td} and P_{tu} are determined only by T and line k always starts at (0, 0). The developed formula for η_{EM} is:

$$\eta_{EM} = \left\{ \left[\frac{a_{II} - a_I}{1 + 0.01\text{^}\left(n - n_m\right)} + a_I \right] \cdot \left| n - n_m \right|\text{^} \left[\frac{2 - p_I}{1 + 0.01\text{^}\left(n - n_m\right)} + p_I \right] + \eta_m \right\} \cdot \left[\frac{2}{1 + 0.01\text{^}\left(n / n_k\right)} - 1 \right] \tag{62}$$

where the variables depending on T are:

$$n_k = \frac{n_{P6}}{T_{P6}} \cdot T \tag{63}$$

$$n_t = \frac{n_{P5} - n_{P4}}{T_{P5}} \cdot T + n_{P4} \tag{64}$$

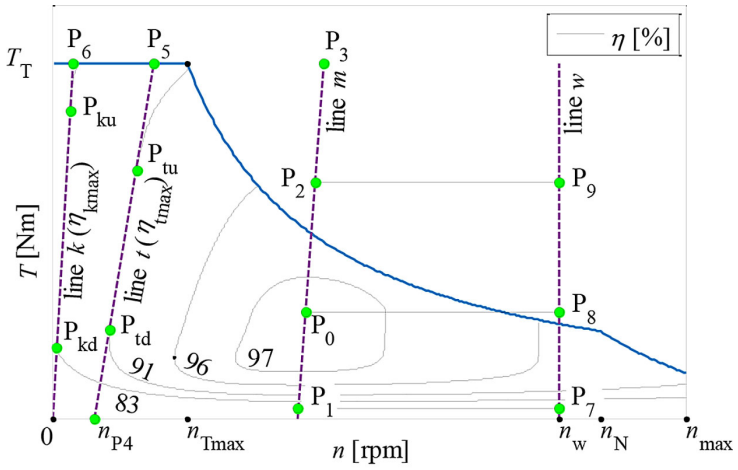

Figure 7. EM efficiency characteristic

$$n_{\mathrm{m}} = \frac{n_{\mathrm{P0}} - n_{\mathrm{P1}}}{T_{\mathrm{P0}}} \cdot T + n_{\mathrm{P1}} \tag{65}$$

$$\eta_{\mathrm{k}} = \eta_{\mathrm{kmax}} \cdot \left[\frac{2}{1 + 0.01\hat{}(T / T_{\mathrm{kd}})} - 1 \right] \cdot \left[\frac{2 \cdot (\eta_{\mathrm{P6}} / \eta_{\mathrm{k\,max}} - 1)}{1 + 0.01\hat{}\left[(T - T_{\mathrm{T}}) / (T_{\mathrm{T}} - T_{\mathrm{ku}}) \right]} + 1 \right] \tag{66}$$

$$\eta_{\mathrm{t}} = \eta_{\mathrm{tmax}} \cdot \left[\frac{2}{1 + 0.01\hat{}(T / T_{\mathrm{td}})} - 1 \right] \cdot \left[\frac{2 \cdot (\eta_{\mathrm{P5}} / \eta_{\mathrm{t\,max}} - 1)}{1 + 0.01\hat{}\left[(T - T_{\mathrm{T}}) / (T_{\mathrm{T}} - T_{\mathrm{tu}}) \right]} + 1 \right] \tag{67}$$

$$\eta_{\mathrm{m}} = \left[\frac{a_{22} - a_{11}}{1 + 0.01\hat{}(T - T_{\mathrm{P0}})} + a_{11} \right] \cdot |T - T_{\mathrm{P0}}| \hat{} \left[\frac{pw_{22} - pw_{11}}{1 + 0.01\hat{}(T - T_{\mathrm{P0}})} + pw_{11} \right] + \eta_{\mathrm{P0}} \tag{68}$$

$$\eta_{\mathrm{w}} = \eta_{\mathrm{m}} \frac{\eta_{\mathrm{P8}}}{\eta_{\mathrm{P0}}} \left[1 + \left(\frac{\eta_{\mathrm{P0}} \eta_{\mathrm{P7}}}{\eta_{\mathrm{P1}} \eta_{\mathrm{P8}}} - 1 \right) \left(\frac{-5}{T_{\mathrm{P7}}^2} + 1 \right) \hat{} (T - T_{\mathrm{P7}})^2 \right] \left\{ \frac{2 \cdot \left[(\eta_{\mathrm{P0}} \eta_{\mathrm{P9}}) / (\eta_{\mathrm{P2}} \eta_{\mathrm{P8}}) - 1 \right]}{1 + 0.01\hat{}\left[(T - T_{\mathrm{P9}}) / (T_{\mathrm{P9}} - T_{\mathrm{P8}}) \right]} + 1 \right\} \tag{69}$$

$$p_{\mathrm{I}} = \frac{\ln\left[(\eta_{\mathrm{t}} - \eta_{\mathrm{m}}) / (\eta_{\mathrm{k}} - \eta_{\mathrm{m}}) \right]}{\ln\left[(n_{\mathrm{t}} - n_{\mathrm{m}}) / (n_{\mathrm{k}} - n_{\mathrm{m}}) \right]} \tag{70}$$

$$a_{\mathrm{I}} = \frac{\eta_{\mathrm{k}} - \eta_{\mathrm{m}}}{|n_{\mathrm{k}} - n_{\mathrm{m}}| \hat{} \, p_{\mathrm{I}}} \tag{71}$$

$$a_{\mathrm{II}} = \frac{\eta_{\mathrm{w}} - \eta_{\mathrm{m}}}{(n_{\mathrm{w}} - n_{\mathrm{m}})^2} \tag{72}$$

and the constant values:

$$pw_{11} = \frac{\ln\left[\eta_{\mathrm{P0}} / (\eta_{\mathrm{P0}} - \eta_{\mathrm{P1}}) \right]}{\ln\left[T_{\mathrm{P0}} / (T_{\mathrm{P0}} - T_{\mathrm{P1}}) \right]} \tag{73}$$

$$a_{11} = \frac{\eta_{\mathrm{P1}} - \eta_{\mathrm{P0}}}{(T_{\mathrm{P0}} - T_{\mathrm{P1}}) \hat{} \, pw_{11}} \tag{74}$$

$$pw_{22} = \frac{\ln\left[(\eta_{\mathrm{P3}} - \eta_{\mathrm{P0}}) / (\eta_{\mathrm{P2}} - \eta_{\mathrm{P0}}) \right]}{\ln\left[(T_{\mathrm{P3}} - T_{\mathrm{P0}}) / (T_{\mathrm{P2}} - T_{\mathrm{P0}}) \right]} \tag{75}$$

$$a_{22} = \frac{\eta_{\mathrm{P2}} - \eta_{\mathrm{P0}}}{(T_{\mathrm{P2}} - T_{\mathrm{P0}}) \hat{} \, pw_{22}} \tag{76}$$

The above formulas allow the efficiency in static states to be determined. In dynamic states, the inertia must be taken into account. The presented model (62) is now compared with the efficiency characteristics of real EMs. The results are presented in Table 7. The EM efficiency model (62) needs more points than the ICE model, because in the case of EMs, often realizing the function of traction EMs, working operating points may constantly occur in the whole working area.

Table 7. Comparison of serial efficiency characteristics with their models based on (62)

	Nissan Kicks	Toyota Prius	Honda Accord
Serial	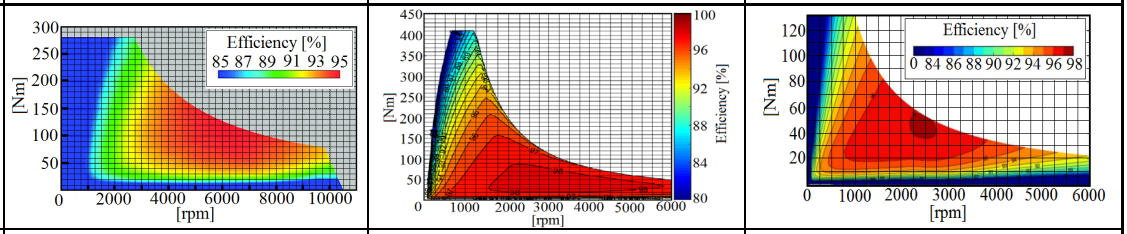		
Model	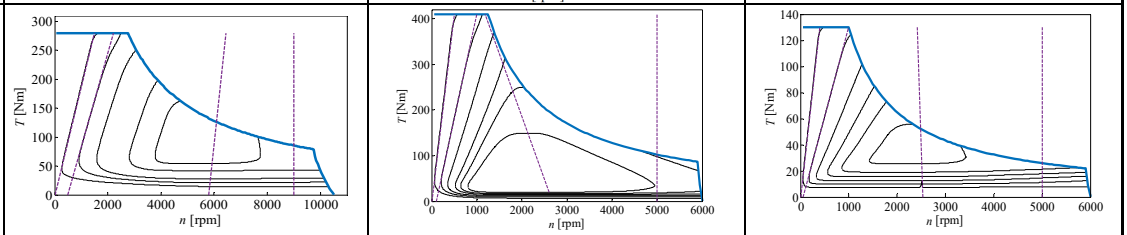		
Δ [%]	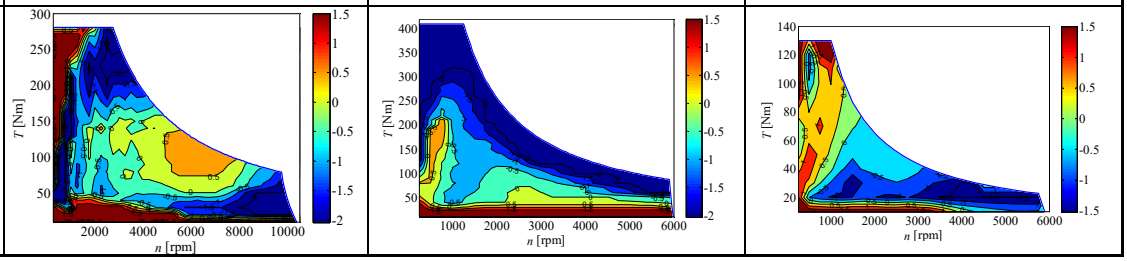		

The results presented in Table 7 show a strong correlation between the models and real characteristics. $|\Delta| < 2\%$ is reached for any work point throughout the whole range of n and T.

Dynamic states

In dynamic states, the EM rotor inertia J_{EM} [kg·m^2] generates additional torque, which influences the dynamic torque T_{dyn}:

$$T_{dyn} = T - J_{EM} \cdot \varepsilon_{EM} \tag{77}$$

where: J_{EM} can be calculated with the use of the developed formula:

$$J_{EM} = 0.001 \cdot \left(0.125 \cdot T_T + 3.75\right) \tag{78}$$

The EM operates with high angular acceleration exceeding 1000 rad/s^2, which may consume over 10% of the total EM torque.

EM start

When the EM starts the ICE it overcomes both ICE inertia as well as its own inertia, which requires the power:

$$P_{\text{EM\_start}} = \frac{T_{\text{EM\_start}} \cdot n_{\text{idle}} \cdot i_{\text{EM\_ICE}}}{9550} = \frac{J_{\text{EM}} \cdot \varepsilon_{\text{EM}} \cdot n_{\text{idle}} \cdot i_{\text{EM\_ICE}}}{9550} \tag{79}$$

INVERTER CHARACTERISTIC

The INV changes the parameters of electric power (voltage and current) and converts direct current from the BAT to alternating current propelling the EM, or vice versa. The INV efficiency η_{INV} depends on the power transferred P^{rel} (Fig. 8). The developed formula that allows the η_{INV} to be calculated is:

$$\eta_{\text{INV}}(P^{\text{rel}}) = -a_0 \cdot \left| P^{\text{rel}} - P_{\text{P0}}^{\text{rel}} \right| \wedge p_0 + \eta_{\text{P0}} \tag{80}$$

where: P^{rel} is the ratio of the actual power transmitted by the INV to its nominal power (which is the nominal power of the relevant EM). The variables are the following:

$$p_0 = \frac{-p}{1 + 0.01 \wedge (P^{\text{rel}} - P_{\text{P0}}^{\text{rel}})} + 2 \cdot p \tag{81}$$

$$a_0 = \frac{(\eta_{\text{P0}} - \eta_{\text{P100}}) / (100 - P_{\text{P0}}^{\text{rel}}) \wedge p_0 - \eta_{\text{P0}} / (P_{\text{P0}}^{\text{rel}}) \wedge p_0}{1 + 0.01 \wedge (P^{\text{rel}} - P_{\text{P0}}^{\text{rel}})} + \frac{\eta_{\text{P0}}}{(P_{\text{P0}}^{\text{rel}}) \wedge p_0} \tag{82}$$

where: p = 2-3.

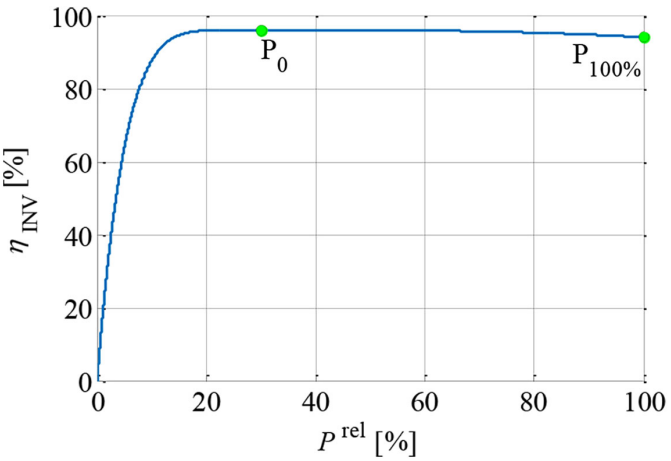

Figure 8. Inverter efficiency vs relative transferred power

BATTERY IN A HYBRID DRIVETRAIN

Battery – general overview

A BAT in a hybrid drivetrain has multiple tasks: it realizes the ICE stop-start function, enables the vehicle to move in an electric mode, recuperates kinetic energy, supports the ICE or accumulates excess energy from the ICE. A properly-sized BAT allows gentle city driving in the electric mode without the assistance of the ICE. This can be assessed based on the WLTP vehicle speed profile, where moderate acceleration in average city traffic is 0.8–1.1 m/s^2 to the speed of 40–45 km/h (the product of $a_v \cdot v < 30$). The required BAT power P_{BAT} [kW] which allows vehicle propulsion is:

$$P_{\text{BAT(Crate\_int)}} = \frac{m_{\text{t}} \cdot \delta \cdot a_{\text{v}} \cdot (v / 3.6)}{1000 \cdot \eta_{\text{tr}} \cdot \eta_{\text{INV}}} \approx 0.01 \cdot m_{\text{t}} \tag{83}$$

This power can be developed during intermittent working conditions lasting 15–20 s. The nominal voltage usually exceeds 180 V and in the case of series design is the sum of each cell voltage.

The parameters of a single cell are: nominal voltage U_{nom} [V], rated capacity RC [Ah], C_{rate_max} [1/h] expressing charge/discharge intensity and internal resistance of a lithium-ion cell R [Ω]. (Figure 9) is based on [30, 70–75]).

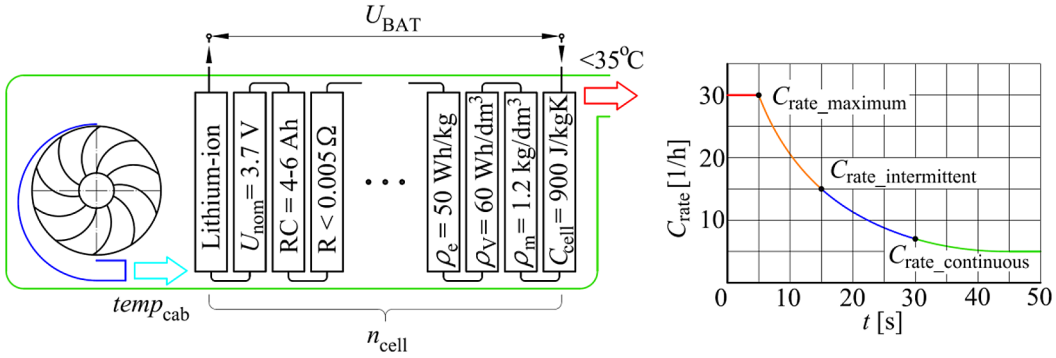

Figure 9. BAT parameters

The BAT parameters are:

$$P_{BAT(Crate)} = P_{cell} \cdot n_{cell} = 0.001 \cdot C_{rate} \cdot RC \cdot \left[U_0(\psi) - R \cdot C_{rate} \cdot RC\right] \cdot n_{cell} \tag{84}$$

$$CAP = 0.001 \cdot n_{cell} \cdot U_{nom} \cdot RC \tag{85}$$

Total capacity CAP [kWh] in a full-hybrid drivetrain varies from 0.9 to 2.4 kWh.

Single cell voltage vs degree of discharge characteristics

For a detailed analysis of the charge and discharge process, the voltage U vs degree of discharge ψ [%] (ψ = 100% − state of charge SOC [%]) characteristic, presented in Figure 10, can be used.

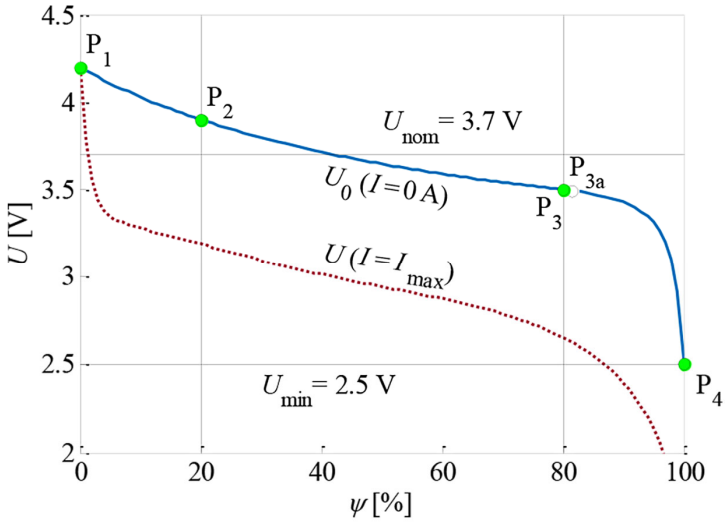

Figure 10. U vs ψ of a lithium-ion cell

The upper blue line represents the characteristic U_0 when no current draws through the cell. The bottom red line represents cell voltage when it provides the maximum current I_{max}. To describe the characteristic of U_0 versus ψ the following formula was developed:

$$U_0(\psi) = \begin{cases} U_{P1} - \psi \cdot k_1 / (\psi + a_1) & \text{for } \psi < \psi_{P3} \\ U_{P4} + (100 - \psi) \cdot k_2 / (100 - \psi + a_2) & \text{for } \psi \geq \psi_{P3} \end{cases} \tag{86}$$

where:

$$a_1 = \frac{\psi_{P2} \cdot \psi_{P3} \cdot (U_{P2} - U_{P3})}{\psi_{P2} \cdot (U_{P3} - U_{P1}) - \psi_{P3} \cdot (U_{P2} - U_{P1})} \tag{87}$$

$$k_1 = (U_{P1} - U_{P2}) \cdot (1 + a_1 / \psi_{P2}) \tag{88}$$

$$\psi_{P3a} = 1.01 \cdot \psi_{P3} \tag{89}$$

$$U_{P3a} = U_{P1} - \psi_{P3a} \cdot k_1 / (\psi_{P3a} + a_1) \tag{90}$$

$$a_2 = \frac{(100 - \psi_{P3a}) \cdot (100 - \psi_{P3}) \cdot (U_{P3} - U_{P3a})}{(100 - \psi_{P3}) \cdot (U_{P3a} - U_{P4}) - (100 - \psi_{P3a}) \cdot (U_{P3} - U_{P4})} \tag{91}$$

$$k_2 = (U_{P3} - U_{P4}) \cdot [1 + a_2 / (100 - \psi_{P3})] \tag{92}$$

To draw the characteristic of U_0, four points must be determined: P_1, P_2, P_3 and P_4. Table 8 presents a comparison of serial $U(\psi)$ characteristics with corresponding models based on (86).

Table 8. Comparison of serial voltage characteristics with their models based on (86)

Parameter	LIR 18650	LG Chem 18650	Panasonic NCR 18650B
Serial	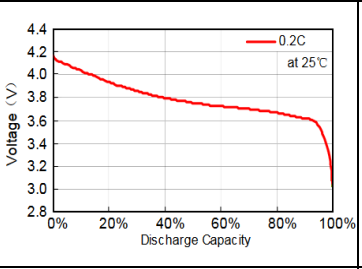	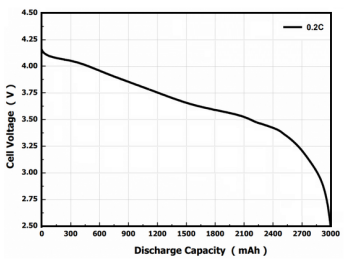	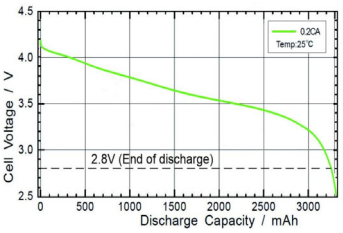
Model	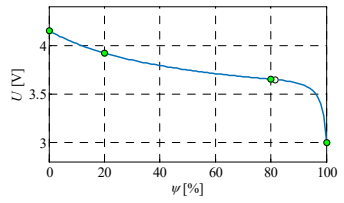	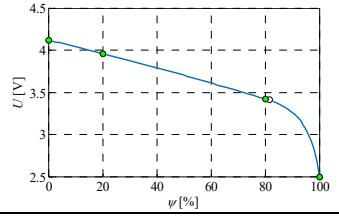	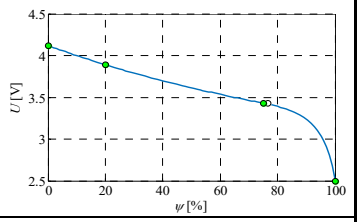
Δ [%]	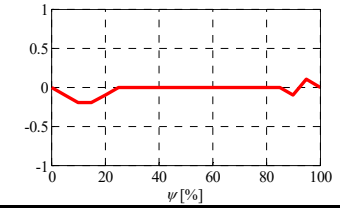	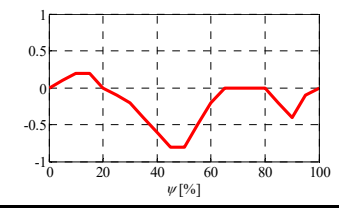	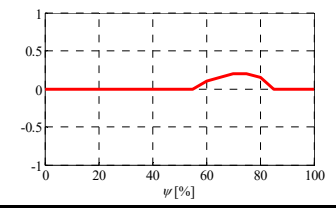

The differences |Δ| presented in Table 8 do not exceed 0.8% in any case. This proves the high accuracy of model (86). To obtain a full voltage characteristic, for different currents and temperatures, the R must also be known. Figure 11 presents R vs ψ for a lithium-ion cell at different working temperatures [29–31, 76]. There is an additional point P_0 with corresponding R_{P0} (minimum value of R). The internal resistance R^{25} of a single cell at 25 °C is:

$$R^{25}(\psi) = \left[\frac{R_{P4} - R_{P1}}{1 + 0.01\text{^}(\psi - \psi_{P0})} + R_{P1} - R_{P0}\right] \cdot \left|\frac{\psi - \psi_{P0}}{\frac{100 - 2 \cdot \psi_{P0}}{1 + 0.01\text{^}(\psi - \psi_{P0})} + \psi_{P0}}\right| \text{^} \left[\frac{p_2 - p_1}{1 + 0.01\text{^}(\psi - \psi_{P0})} + p_1\right] + R_{P0} \tag{93}$$

where:

$$p_1 = \log[(R_{P2} - R_{P0})/(R_{P1} - R_{P0})] / \log[(\psi_{P0} - \psi_{P2})/\psi_{P0}] \tag{94}$$

$$p_2 = \log[(R_{P3} - R_{P0})/(R_{P4} - R_{P0})] / \log[(\psi_{P3} - \psi_{P0})/(100 - \psi_{P0})] \tag{95}$$

At low temperatures, cell performance deteriorates due to increased R. The developed dimensionless coefficient C_R (varies from $C_R = 3$ for −10 °C to $C_R = 0.5$ at 50 °C) represents the change of cell R in relation to its temperature:

$$C_R = 2.2 \cdot 0.969 \hat{} temp_{cell} \tag{96}$$

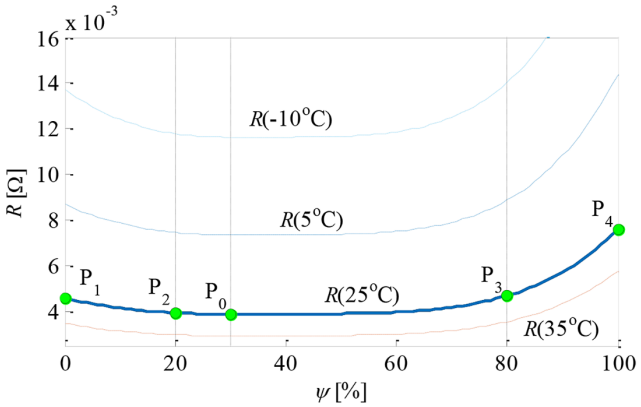

Figure 11. Resistance vs degree of discharge for a lithium-ion cell

Finally, the formula for R, in the temperature range −10–50 °C, is:

$$R = R^{25} \cdot C_R \tag{97}$$

To perform in the area of the lowest internal resistance R level (high efficiency and low temperature gradients) and extend the lifetime of a lithium-ion battery, their *SOC* should operate within the maximum range of (30–80%)·*CAP*. Moreover, the BAT must always be ready for an e-boost and recharging. This means that the *SOC* should vary only by 25%·*CAP*.

Battery thermal behaviour

The simplified model of uniform thermal behaviour of a cell is:

$$\Delta temp_{cell} = \left\{ 0.001 \cdot N_{cell} \cdot \left[1 - \left(\frac{U_0(\psi)}{U_0(\psi) + k_c \cdot I \cdot R} \right)^{k_c} \right] - h_{air} \cdot A_{cell} \cdot (t_{cell} - t_{cab}) \right\} \cdot \frac{\Delta t}{C_{cell} \cdot m_{cell}} \tag{98}$$

where: h_{air} = (10–25) W/m^{2}K (smallest value for BAT fan off, largest for fan max speed), t_{cab} is the cabin temperature and $k_c = 1$ for BAT charging and $k_c = -1$ for BAT discharging. Part of the Equation 98 in round brackets represents the efficiency of charging and discharging and is used in power losses calculations.

VALIDATION OF HYBRID TRANSMISSION MODELS

In this section, a design example of a Hyundai Ioniq parallel hybrid is used to present drivetrain parameters in a WLTP test from the simulation model. Parameters of this vehicle are the following: $V_{ICE} = 1.6$ dm^3, $P_N = 77$ kW, $n_N = 5700$ rpm, $T_T = 147$ Nm, $n_T = 4000$ rpm, $CAP = 1.6$ kWh, $P_{EM} = 32$ kW, $m_e = 1436$ kg.

The simulation model utilizes control strategies that make the ICE work only in the area of its highest efficiency: when resistances are small the ICE is additionally loaded by the EM and charges the BAT, whereas when resistances are high the ICE is supported by the EM powered by the BAT.

The first simulation is based on a WLTP homologation cycle. Selected parameters of the drivetrain are presented in Figure 12. In the case of the WLTP test, BAT temperature increases by 6 °C from 25 °C to 31 °C, which is less than 35 °C (safe limit for lifetime durability of the BAT). In [77] an increase of 8 °C was obtained

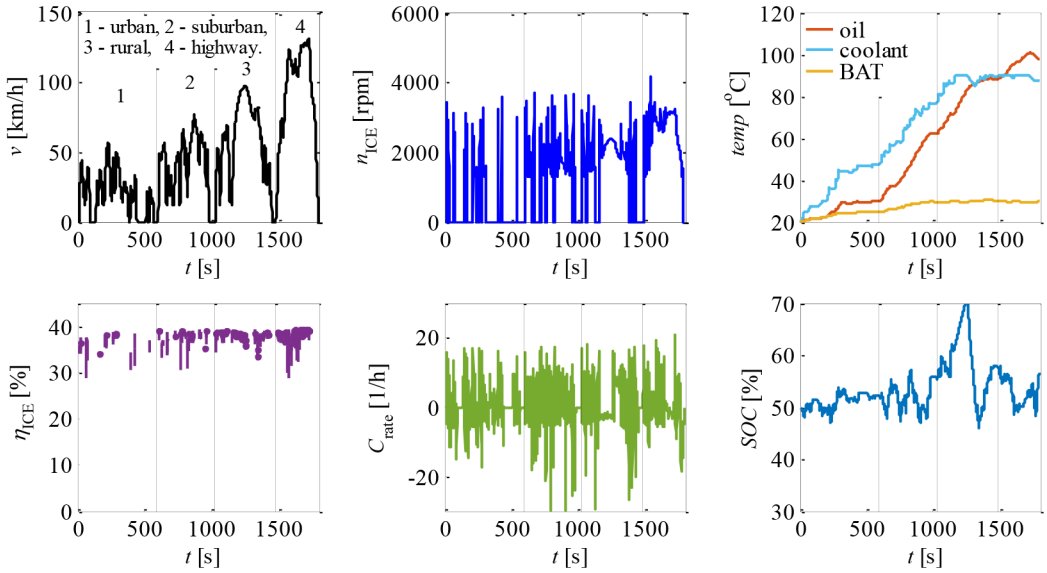

Figure 12. Drivetrain parameters of a Hyundai Ioniq hybrid in a WLTP homologation test

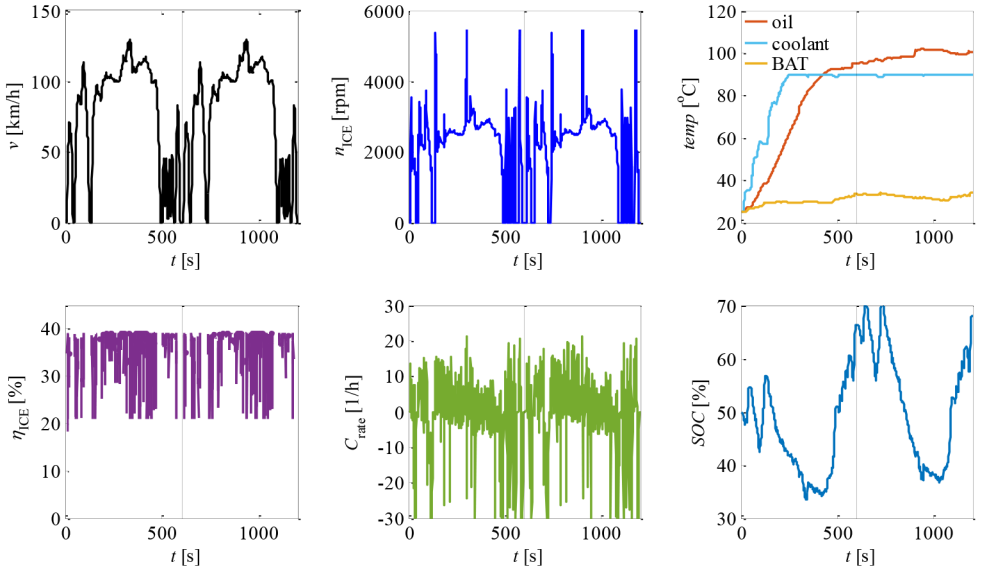

Figure 13. Drivetrain parameters in two subsequent US06 homologation tests

in WLTP for a vehicle of similar size. *SOC* varies in the range 45–70% which is 25%·*CAP*. Similar *SOC* ranges were obtained in [78], [79] and [80]: 18%·*CAP*, 28%·*CAP* and (20–25%)·*CAP*, respectively. As a result of this simulation, G_V = 4.35 dm^3/100 km for the considered vehicle is obtained. For the serial vehicle fuel consumption is 4.40 dm^3/100km.

The second simulation is conducted for a double US06 homologation cycle, which is a high acceleration aggressive driving schedule that is often identified as the Supplemental Federal Test Procedure driving schedule. The results are presented in Figure 13.

In the US06 test, which is characterized by continuous strong dynamic states, BAT charging and discharging phases occur frequently and its temperature rises 8 °C from 25 °C to 33 °C, which is only 2 °C more than in WLTP, and still remains in a safe range. Due to strong and long e-boost phases, the *SOC* varies by 35%·*CAP*, which is 10% more than in WLTP. The average fuel consumption is G_v = 7.8 dm^3/100 km. ICE thermal behaviour (in WLTP and US06) is verified by comparing its temperature increases in short subsequent time intervals with regard to its speed and torque, with reference measurements [52, 81–84]. A comparison indicates a ± 8% difference depending on the ICE operating conditions.

CONCLUSIONS

The comparisons of single characteristics with production ones indicate:

- > 98% average accuracy for ICE torque characteristic.
- > 95% average accuracy for ICE efficiency characteristic.
- > 98% absolute accuracy for EM efficiency characteristic.
- > 99% absolute accuracy for BAT voltage characteristic.

Performed simulations of drivetrain performance in WLTP and US06 homologation tests indicate:

- The ICE thermal characteristic differs less than 8% from values indicated in other research. This concerns low-speed and high-speed driving, as well as low and high dynamics.
- The recommended range of the C_{rate} parameter and *SOC* allows the BAT temperature to be maintained below 35 °C (with the cabin temperature of 25 °C).
- ICE efficiency varies in the high range of 20–40% in each simulation, which also proves the suitability of the implemented control algorithm.

The proposed characteristics, with recommended parameter ranges, may be applied to any transmission design: series, parallel or series-parallel with planetary gears. The proposed models allow the warm-up period to be included, which influences fuel consumption significantly, especially over short distances. The provided formulas can be implemented in any program, thus they can be useful for students, scientists, engineers and enthusiasts in this area searching for more technical information on hybrids.

Acknowledgement

This work was supported by the AGH University of Krakow, Faculty of Mechanical Engineering and Robotics [Research program No. 16.16.130.942 / B403 KPiEM].

REFERENCES

[1] Dornoff J. CO_2 emission standards for new passenger cars and vans in the European Union. International Council on Clean Transportation. May 2023.

[2] Bielaczyc P., Woodburn J., Joshi A.A. Worldwide trends in powertrain system development in light of emissions legislation, fuels, lubricants and test methods. Combustion Engines 2021, 184(1), 57–71. https://doi.org/10.19206/CE-134785

[3] ACEA Position Paper, Views on proposals for Euro 7 emission standard. European Automobile Manufacturers Association. December 2020.

[4] ICCT's comments and technical recommendations on future Euro 7 emission standards. The International Council of Clean Transportation. Berlin, May 7, 2021.

[5] Carney D. Toyota unveils more new gasoline ICEs with 40% thermal efficiency. SAE International. April 2018.

[6] Wong V.W., Tung S.C. Overview of automotive engine friction and reduction trends – effects of surface, material, and lubricant-additive technologies. Friction 2016, 4(1), 1–28. https://doi.org/10.1007/s40544-016-0107-9

[7] Ding H., Cai C., Chen Z., Ke T., Mao B. Configuration synthesis and performance analysis of 9Speed automatic transmissions, Chinese Journal of Mechanical Engineering, June 2020. https://doi.org/10.1186/s10033-020-00466-y

[8] Yadav P., Shinde A., Gangurde Y., Patil P. Review on weight reduction in automobile, International Journal of Advanced Technology in Engineering and Science 2016, 4(1).

[9] Mukut A.N.M.M.I., Abedin M.Z. Review on aerodynamics drag reduction of vehicles. International Journal of Engineering Materials and Manufacture 2019, 4(1), 1–14. https://doi.org/10.26776/ijemm.04.01.2019.01

[10] Sanguesa J.A., Torres-Sanz V., Garrido P., Martinez F.J., Marquez-Barja J.M. A review on electric vehicles: technologies and challenges. Smart Cities 2021, 4, 372–404. https://doi.org/10.3390/smartcities4010022

[11] Haddad A., Mannah M., Bazzi H. Nonlinear time-variant model of the PEM type fuel cell for automotive applications. Simulation Modelling Practice and Theory 2015, 51, 31–44. https://doi.org/10.1016/j.simpat.2014.11.002

[12] Rahma M.M., Kamil M., Bakar R.A. Engine performance and optimum injection timing for 4-cylinder direct injection hydrogen fueled engine. Simulation Modelling Practice and Theory 2011, 19, 734–751. https://doi.org/10.1016/jsimpat.2010.10.006

[13] Pevec D., Babic J., Carvalho A. Electric Vehicle Range Anxiety: An obstacle for the personal transportation Ievolution? 4th International Conference on Smart and Sustainable Technologies

(SpliTech), 2019. https://doi.org/10.23919/SpliTech.2019.8783178

[14] Seitaridis A., Rigas E.S., Bassiliades N., Ramchurn S.D. An agent-based negotiation scheme for the distribution of electric vehicles across a set of charging stations. Simulation Modelling Practice and Theory 2020, 100. https://doi.org/10.1016/j.simpat.2019.102040

[15] Gómez Vilchez J.J., Smyth A., Kelleher L., Lu H., Rohr C., Harrison G., Thiel C. Electric car purchase price as a factor determining consumers' choice and their views on incentives in Europe. Sustainability 2019, 11(22), 6357. https://doi.org/10.3390/su11226357

[16] Ma S., Jiang M., Tao P., Song C., Wu J., Wang J., Deng T., Shang W. Temperature effect and thermal impact in lithium-ion batteries: A review. Progress in Natural Science: Materials International 2018, 28(6), 653–666. https://doi.org/10.1016/j.pnsc.2018.11.002

[17] Ruiz V. Standards for the performance and durability assessment of electric vehicle batteries. Publications Office of the European Union, Luxembourg, 2018. https://doi.org/10.2760/24743 JRC113420.

[18] Haque N., Hughes A., Lim S., Vernon C. Rare earth elements: Overview of mining, mineralogy, uses, sustainability and environmental impact. Resources 2014, 3, 614–635. https://doi.org/0.3390/resources3040614

[19] Panagopoulos A.A., Christianos F., Katsigiannis M., Mykoniatis K., Chalkiadakis G., Pritoni M., Peffer T., Panagopoulos O.P., Rigas E.S., Culler D.E., Jennings N.R., Lipman T. iPlugie: Intelligent electric vehicle charging in buildings with grid-connected intermittent energy resources. Simulation Modelling Practice and Theory 2022, 115. https://doi.org/10.1016/j.simpat.2021.102439

[20] Wang Y., Haifeng S., Wenhao W., Yunjing Z. The impact of electric vehicle charging on grid reliability. IOP Conf. Ser.: Earth Environ. Sci. 2018, 199, 052033. https://doi.org/10.1088/1755-1315/199/5/052033

[21] Asif U., Schmidt K. Fuel cell electric vehicles (FCEV): Policy advances to enhance commercial success. Sustainability 2021, 13(9), 5149. https://doi.org/10.3390/su13095149

[22] Ju F., Murgovski N., Zhuang W., Hu X. Predictive energy management with engine switching control for hybrid electric vehicle via ADMM, Energy 2022, 263(1), 125971. https://doi.org/10.1016/j.energy.2022.125971

[23] Han L., Yang K., Ma T., Yang N., Liu H., Guo L. Battery life constrained real-time energy management strategy for hybrid electric vehicles based on reinforcement learning. Energy 2022, 259, 124986. https://doi.org/ 10.1016/j.energy.2022.124986

[24] Zhuang W., Li (Eben) S., Zhang X., Kum D., Song Z., Yin G., Ju F. A survey of powertrain configuration studies on hybrid electric vehicles. Applied Energy 2020, 262, 114553. https://doi.org/10.1016/j.apenergy.2020.114553

[25] Wei D., He H., Cao J. Hybrid electric vehicle electric motors for optimum energy efficiency: A computationally efficient design. Energy 2020, 203, 117779. https://doi.org/10.1016/j.energy.2020.117779

[26] Zhang F., Xiao L., Coskun S., Pang H., Xie S., Liu K., Cui Y. Comparative study of energy management in parallel hybrid electric vehicles considering battery ageing. Energy 2022, 264, 123219. https://doi.org/ 10.1016/j.energy.2022.123219

[27] Pielecha I., Cieślik W., Fluder K. Analysis of energy management strategies for hybrid electric vehicles in urban driving conditions. Combustion Engines 2018, 173(2), 14–18. https://doi.org/10.19206/CE-2018-203

[28] Wang H., Zhang X., Ouyang M. Energy consumption of electric vehicles based on real-world driving patterns: A case study of Beijing. Applied Energy 2015, 157, 710–719. https://doi.org/10.1016/j.apenergy.2015.05.057

[29] Singh A., Obaidat M. S., Singh S., Aggarwal A., Kaur K., Sadoun B., Kumar M., Hsiao K-F. A simulation model to reduce the fuel consumption through efficient road traffic modelling. Simulation Modelling Practice and Theory 2022, 121. https://doi.org/10.1016/j.simpat.2022.102658

[30] Kleiner J., Komsiyska L., Elger G., Endisch C. thermal modelling of a prismatic lithium-ion cell in a battery electric vehicle environment: influences of the experimental validation setup. Energies 2020, 13(1). https://doi.org/10.3390/en13010062

[31] Aris A.M., Shabani B. An experimental study of a lithium ion cell operation at low temperature conditions. Energy Procedia 2017, 110, 128–135. https://doi.org/10.1016/j.egypro.2017.03.117

[32] Mahmud A.H., Daud Z.H.C., Asus Z. The impact of battery operating temperature and state of charge on the lithium-ion battery internal resistance. Jurnal Mekanikal 2017, 40, 1–8.

[33] Ehsani M., Gao Y., Longo S., Ebrahim K. Modern electric, hybrid electric, and fuel cell vehicles. CRC Press, Taylor&Francis Group, 2018.

[34] Lechner G., Naunheimer H. Automotive transmissions: Fundamentals, selection, design and application, Springer-Verlag Berlin Heidelberger, Germany, 1999.

[35] Siłka W., Teoria ruchu pojazdu (in Polish). WNT, Warszawa, 2002.

[36] Bera P. A design method of selecting gear ratios in manual transmissions of modern passenger cars. Mechanism and Machine Theory 2019, 132. 133–153, https://doi.org/10.1016/j.mechmachtheory.2018.10.013

[37] Jaśkiewicz Z. Obliczanie układów napędowych (in Polish), WKiŁ 1972, Warszawa.

[38] Sauleda F. Automotive clutch facings. Material G95. E-08396 Sant Cebrià de Vallalta, Barcelona, Spain, 2020.

[39] Stopp R., Siefert C., 7th LuK Symposium, 11-12.04.2002, Germany, GMBH, LuK Symposium.

[40] Husain I. Electric and hybrid vehicles, design fundamentals. CRC Press, Taylor&Francis Group.

[41] Crolla D., Foster D., Kobayashi T., Vaughan N. Encyclopedia of automotive engineering. John Wiley & Sons 2015, 886–887.

[42] Ju F., Zhuang W., Wang L., Zhang Z. Optimal sizing and adaptive energy management of a novel fur-wheel-drive hybrid powertrain. Energy 2019, 187, 116008, https://doi.org/10.1016/j.energy.2019.116008

[43] Wajand J.A., Wajand J.T. Tłokowe silniki spalinowe średnio- i szybkoobrotowe (in Polish). WNT 2005.

[44] Bera P. Torque characteristic of SI engine in dynamic operating states. Combustion Engines 2017, 171(4), 175–180. https://doi.org/10.19206/CE-2017-429

[45] Bera P. Development of engine efficiency characteristic in dynamic working states. Energies 2019, 12, 2906. https://doi.org/10.3390/en12152906

[46] Shaolin Q., Lihong Q., Lijun Q. Hierarchical energy management control strategies for connected hybrid electric vehicles considering efficiencies feedback. Simulation Modelling Practice and Theory 2019, 90, 1–15. https://doi.org/10.1016/j.simpat.2018.10.008

[47] Liu Y., Wu Y., Wang X., Li L., Zhang Y., Chen Z. Energy management for hybrid electric vehicles based on imitation reinforcement learning. Energy 2023, 263(C), 125890. https://doi.org/10.1016/j.energy.2022.125890

[48] Heywood J.B. Internal Combustion Engine Fundamentals. McGaw-Hill, Inc., United States of America, 1988.

[49] Razmara M., Bidarvatan M., Shahbakhti M., Robinett III R. D. Optimal exergy-based control of internal combustion engines. Applied Energy 2016, 183, 1389–1403. https://doi.org/10.1016/j.apenergy.2016.09.058

[50] Roberts A., Brooks R., Shipway P. Internal combustion engine cold-start efficiency: A review of the problem, causes and potential solutions. Energy Conversion and Management 2014, 82, 327–350. https://doi.org/10.1016/j.enconman.2014.03.002

[51] Cipollone R., Di Battista D., Mauriello M.M. Effects of oil warm up acceleration on the fuel consumption of reciprocating internal combustion engines. Energy Procedia 2015, 82, 1–8. https://doi.org/10.1016/j.egypro.2015.11.870

[52] Trapy J.D., Damiral P. An investigation of lubricating system warm-up for the improvement of cold start efficiency and emissions of S.I. automotive engines, SAE Transactions 1990, 99(6), Journal of passenger cars, 1635–1645.

[53] Di Battista D., Cipollone R. Experimental and numerical assessment of methods to reduce warm up time of engine lubricant oil. Applied Energy 2016, 162, 570–580. https://doi.org/10.1016/j.apenergy.2015.10.127

[54] Derbiszewski B., Woźniak M., Grala Ł., Waleciak M., Hryshchuk M., Siczek K., Obraniak A., Kubiak P. A study on the flow resistance of fluids flowing in the engine oil-cooler chosen. Lubricants 2021, 9(8). https://doi.org/10.3390/lubricants9080075

[55] PáV K., Rychtář V., Vorel V. Heat balance in modern automotive engines. Škoda Auto a.s., Mladá Boleslav 293 60, Mecca 02 2012. https://doi.org/10.2478/v10138-012-0007-7

[56] Rundo M., Nervegna N. Lubrication pumps for internal combustion engines: a review. International Journal of Fluid Power 2015, 16(2), 59–74. https://doi.org/ 10.1080/14399776.2015.1050935

[57] Liu F. Analysis of BJ493 diesel engine lubrication system properties. IOP Conf. Series: Materials Science and Engineering 2017, 283. https://doi.org/10.1088/1757-899X/283/1/012005

[58] Oil pumps for internal combustion engines and transmissions. Conventional, Variable and Electrical. Pierburg pump technology GmbH 2012, Alfred Pierburg StraBe, 41460 Neuss, Germany.

[59] Temperature-controlled lubricating oil pumps save fuel, 7th LuK Symposium, 11/12 April 2002, LuK GmbH & Co, Industriestrasse 3, D-77815 Buhl/Baden.

[60] Rahmani R., Rahnejat H., Fitzsimons B., Dowson D. The effect of cylinder liner operating temperature on frictional loss and engine emissions in piston ring conjunction. Applied Energy 2017, 191, 568–581. https://doi.org/10.1016/j.apenergy.2017.01.098

[61] Shimada A., Harigaya Y., Suzuki M., Takiguchi M. An Analysis of Oil Film Temperature, Oil Film Thickness and Heat Transfer on a Piston Ring of Internal Combustion Engine: The Effect of Local Lubricant Viscosity. SAE 2004-32-0024, JSAE 20044311. https://doi.org/10.4271/2004-32-0024

[62] Nikolakopoulos P.G., Mavroudis S., Zavos A. Lubrication performance of engine commercial oils with different performance levels: The effect of engine synthetic oil aging on piston ring tribology under real engine conditions. Lubricants 2018, 6(4), 90. https://doi.org/10.3390/lubricants6040090

[63] Sun S., Sun N., Wang X. Study on mixed lubrication characteristics of piston/cylinder interface of variable length. AIP Advances 2019, 9, 075303. https://doi.org/10.1063/1.5093925

[64] Žák Z., Emrich M., Takáts M., Macek J. In-cylinder heat transfer modelling. Mecca 2016, De Gruyter Open. https://doi.org/10.1515/mecdc-2016-0009

[65] Sandoval D., Heywood J. B. An improved friction model for spark-ignition engines. SAE International 2003. https://doi.org/10.4271/2003-01-0725

[66] Jeffrey R.S. Characterization and modelling of rubbing friction in a motored four-cylinder internal combustion engine. Master's Thesis of Applied Science in the Department of Mechanical Engineering, McMaster University, Hamilton, Canada, 2011.

[67] Mobil Super™ Synthetic, Mobil Passenger Vehicle Lube, Exxon Mobil Corporation, 22777 Springwoods Village Parkway, Spring TX 77389.

[68] Dong P., Wu S., Guo W., Xu X. Coordinated clutch slip control for the engine start of vehicles with P2-hybrid automatic transmissions. Mechanism and Machine Theory 2020, 153, 103899. https://doi.org/10.1016/j.mechmachtheory.2020.103899

[69] Huang K.D., Tzeng S.C. A new parallel-type hybrid electric-vehicle. Applied Energy 2004, 79, 51–64. https://doi.org/10.1016/j.apenergy.2003.12.001

[70] Anselma P. G., Kollmeyer P., Lempert J., Zhao Z., Belingardi G., Emadi A. Battery state-of-health sensitive energy management of hybrid electric vehicles: Lifetime prediction and ageing experimental validation. Applied Energy 2021, 285, 116440. https://doi.org/10.1016/j.apenergy.2021.116440.

[71] Emadi A., Advanced electric drive vehicles. CRC Press, Taylor&Francis, 2014.

[72] Maleki H., Al Hallaj S., Selman J.R., Dinwiddie R.B., Wang H. Thermal properties of lithium-ion battery and components. Journal of The Electrochemical Society 1999, 146(3), 947–954. https://doi.org/10.1149/1.1391704

[73] Wang Z., Ma J., Zhang L. Finite element thermal model and simulation for a cylindrical li-ion battery. China National Engineering Laboratory for Electric Vehicles, Beijing Institute of Technology, Beijing 2017, China. https://doi.org/10.1109/ACCESS.2017.2723436

[74] Drage P., Hinteregger M., Zotter G., Šimek M. Cabin conditioning for electric vehicles. ATZ worldwide, 02/2019.

[75] Chen D., Jiang J., Kim G-H., Yang C., Pesaran A. Comparison of different cooling methods for lithium ion battery cells. Applied Thermal Engineering 2016, 94, 846–854. https://doi.org/10.1016/j.applthermaleng.2015.10.015

[76] Groiß R. The influence of temperature on the operation of batteries and other electrochemical energy storage systems, BaSyTec GmbH, Öllinger Weg 17, 89176 Asselfingen, Germany, 2018.

[77] Che Daud Z.H., Asus Z., Abu Bakar S.A., Abu Hasain N., Mazali I.I., Chrenko D. Thermal characteristics of a lithium-ion battery used in a hybrid electric vehicle under various driving cycles. IET Electrical Systems in Transportation 2020, 10(3), 243–248. https://doi.org/10.1049/iet-est.2019.0018

[78] Liu J., Peng H., Filipi Z. Modeling and analysis of the Toyota Hybrid System. Proceedings of the 2005 IEEE/ASME, International Conference on Advanced Intelligent Mechatronics, Monterey, California, USA, 24–28 July.

[79] Cieślik W., Pielecha I., Szałek A. Assessment of parameters of the hybrid drive system in vehicles in urban traffic conditions. Combustion Engines 2015, 161(2), 14–17. https://doi.org/10.19206/CE-116887

[80] Cubito C., Millo F., Boccardo G., Di Pierro G., Ciuffo B., Fontaras G., Serra S., Garcia M.O., Trentadue G. Impact of different driving cycles and operating conditions on CO_2 emissions and energy management strategies of a Euro-6 hybrid electric vehicle. Energies 2017, 10(10), 1590. https://doi.org/10.3390/en10101590

[81] Wang D., Song C., Shao Y., Song S., Peng S., Xiao F. Optimal control strategy for series hybrid electric vehicles in the warm-up process. Energies 2018, 11(5), 1091. https://doi.org/10.3390/en11051091

[82] Koksal H., Ceviz M.A., Yakut K., Kaltakkiran G., Özakin A.N. A novel ignition timing strategy to regulate the energy balance during the warm up phase of an SI engine. Case Studies in Thermal Engineering 2023, 41. https://doi.org/10.1016/j.csite.2022.102602

[83] Ibrahim T.M., Syahir A.Z., Zulkifli N.W.M., Masjuki H.H., Osaman A. Enhancing vehicle's engine warm up using integrated mechanical approach. IOP Conference Series: Materials Science and Engineering 2017, 210, 012064. https://doi.org/10.1088/1757-899X/210/1/012064

[84] Kneba Z. Research on the phenomena of warming up and free cooling down the car engine. IOP Conference Series: Materials Science and Engineering 2018, 421, 042037. https://doi.org/10.1088/1757-899X/421/4/042037